Journal Name

ARTICLE

A Hydride Composite Featuring Mutual Destabilisation and Reversible Boron Exchange: $Ca(BH_4)_2$-Mg_2NiH_4

N. Bergemann,[a] C. Pistidda,[a] C. Milanese,[b] M. Aramini,[c] Huotari, S.[c], P. Nolis,[d] A. Santoru,[a] M. R. Chierotti,[e] A.-L. Chaudhary,[a] M. D. Baro,[f] T. Klassen[a,g], M. Dornheim[a]

Received 00th January 20xx,
Accepted 00th January 20xx

DOI: 10.1039/x0xx00000x

www.rsc.org/

The system Ca(BH4)2-Mg2NiH4 is used as a model to prove the unique possibility to fully reverse the borohydride decomposition process even in cases where the decomposition reaction leads to undesired stable boron containing species (boron sinks). The formation of MgNi2.5B2 directly from Ca(BH4)2 or from CaB12H12 and amorphous boron allows an unexpectedly easy transfer of the boron atoms to reversibly form Ca(BH4)2 during rehydrogenation. In addition, to the best of our knowledge, the mutual destabilisation of the starting reactants is observed for the first time in Ca(BH4)2 based Reactive Hydride Composite (RHC) systems. A detailed account of dehydrogenation and rehydrogenation reaction mechanisms as the function of applied experimental conditions is given.

Introduction

The first indisputable evidences of climate change made many people realise the importance of new concepts for energy generation, distribution and storage. More and more creative solutions of utilising the planet's renewable energy sources are currently being developed or have already reached the market. The typically decentralised infrastructure of renewable energy generation sets the demands for modern smart power grids. Due to the non-continuous power generation of most renewables (e. g. wind energy or solar power), efficient ways of storing excess energy become crucial components in future power grids. With different local conditions and diverse forms of supplying sustainable power into the grid, not just one energy storage solution but several complementary concepts will be required. Besides solutions for mechanical energy storage (e. g. compressed air, flywheels or pumped hydro), electrical energy storage (e. g. batteries, flow batteries, super capacitors or super conducting magnets) and thermal energy storage (e. g. sensible or latent heat storage), also chemical energy storage technologies are promising concepts.[1–4] In this field, hydrogen technology can play a key role. By dissociating water into hydrogen and oxygen, energy obtained from renewable sources is converted into chemical energy. Herein, storing the hydrogen efficiently is the major challenge. Apart from the compression of this gas (to pressures up to 700 bar) and the liquefaction, the integration of hydrogen atoms into solid materials offers great potential.[5–8] During the last two

[a] *Institute of Materials Research, Materials Technology, Helmholtz-Zentrum Geesthacht GmbH, Max-Planck-Straße 1, D-21502, Geesthacht, GermanyAddress here.*
[b] *Pavia Hydrogen Lab, CSGI and Università di Pavia, Dipartimento di Chimica, Sezione di Chimica Fisica, Viale Taramelli, 16, 27100, Pavia, Italy*
[c] *Department of Physics, University of Helsinki, Gustaf Hällströmin katu 2 P.O. Box 64, Helsinki, Finland*
[d] *Servei de Ressonància Magnètica Nuclear, Universitat Autònoma de Barcelona, Cerdanyola del Vallès, Spain*
[e] *Department of Chemistry and NIS Centre, University of Torino, Via P. Giuria 7, Torino, Italy*
[f] *Departament de Física, Facultat de Ciències, Universitat Autònoma de Barcelona, E-08193 Bellaterra, Cerdanyola del Vallès, Barcelona, Spain*
[g] *Helmut Schmidt University, Institute of Materials Technology, Hamburg, Germany*

† Footnotes relating to the title and/or authors should appear here.
Electronic Supplementary Information (ESI) available: [details of any supplementary information available should be included here]. See DOI: 10.1039/x0xx00000x

decades the research on metal hydrides and hydride composites was conducted intensively. The discovery of reversibility in Ti-doped $NaAlH_4$ by Bogdanović et al.[9] in 1997 was a mile stone and the beginning of a series of important findings in the field of hydrogen storage. In 2002, Chen et al.[10] introduced reversible amide/imide based hydrogen storage system and two years later Barkhordarian et al.[11,12] and Vajo et al.[13] reported on $LiBH_4$-MgH_2, the first fully reversible borohydride based composite. Due to their rather high gravimetric hydrogen capacity, light metal borohydrides have been regarded as potential candidates for hydrogen storage applications and hence been thoroughly investigated [14–17]. However, in the last couple of years a certain trend became obvious. Many research groups in the hydrogen community partially moved their focus away from classical hydrogen storage to other hydride-based applications. For instance, the discovery of the excellent ion conductivity of many boro-hydrides or closo-boranes led to increased research efforts for battery applications. The employment of these materials as electrolytes for Li-, Na- and Mg-batteries is explored intensively.[18,19] A growing interest in the application of high temperature metal hydrides for thermal energy storage can also be perceived.[19–22] In addition, the potential to use complex metal borohydrides as active layers of solar cells was emphasised.[22] The reason for this partial renunciation of hydrogen storage research might be explained by unfulfilled expectations. Primary obstacles to the utilization of complex hydrides as hydrogen storage medium such as high dehydrogenation temperatures, slow reaction kinetics, complex desorption paths and the formation of stable byproducts could not be cleared. In the case of $Ca(BH_4)_2$, this is as follows: at a hydrogen capacity of 9.6 mass% and a relatively low thermal stability compared to other light metal borohydrides like e. g. $LiBH_4$ or $NaBH_4$,[23–26] $Ca(BH_4)_2$ seems to be an attractive candidate for mobile hydrogen storage applications. However, upon closer examination, several problems become evident. As reported in the literature, pure $Ca(BH_4)_2$ dehydrogenates along different reaction paths:

1) $Ca(BH_4)_2 \rightarrow CaH_2 + 2B + 3H_2$ [24,27,28]
2) $Ca(BH_4)_2 \rightarrow 2/3CaH_2 + 1/3CaB_6 + 10/3H_2$ [24,27,29–31]
3) $Ca(BH_4)_2 \rightarrow 1/6CaB_{12}H_{12} + 5/6CaH_2 + 13/6H_2$ [30–32]
4) $Ca(BH_4)_2 \rightarrow CaB_2H_6 + H_2$ (intermediate reaction)[27,31,32].

These reaction paths depend on the dehydrogenation conditions, i. e. on external parameters such as temperature, hydrogen pressure or heating rate.[27,32,33] The formation of amorphous boron and $CaB_{12}H_{12}$ was identified to restrict reversibility as these compounds are rather stable.[28,32,33] Although the evolution of these phases can be largely suppressed by limiting the temperature from 320 °C to 350 °C (in vacuum), this approach comes at the expense of highly reduced reaction kinetics.[27,34,35] Also the combination of $Ca(BH_4)_2$ with other materials (i. e. the concept of Reactive Hydride Composites[16]) has not been successful yet: either boron was not transferred to the reaction partner[36–39] or the reaction proved to be irreversible[40,41].

In this paper we show that the utilization of $Ca(BH_4)_2$ as hydrogen storage material is indeed a very promising idea because our results proof that several of the drawbacks can be overcome. We present the Reactive Hydride Composite $Ca(BH_4)_2$-Mg_2NiH_4 that shows the promising features:

1. boron is reversibly exchanged in the sorption process
2. the formation of stable boron sinks is avoided
3. mutual destabilisation of the two hydrides is possible.

Thus, our findings confirm that the drawbacks of borohydrides can be addressed and suitable hydrogen storage systems realised.

Experimental

Details on equipment and experimental parameters

All materials were handled in argon-filled gloveboxes with oxygen and water levels lower than 1 ppm.

Two types of milling devices were employed to prepare fine powders and ensure homogeneously mixed composites. A Fritsch Planetary P6 was used to mill larger amounts of material. Here, the milling was performed either in Al_2O_3 or WC milling vials. For all other material preparations a SPEX SamplePrep 8000 Mill with stainless steel milling vials was employed.

Hydrogenation was carried out in 25 ml autoclaves from Parr Instrument. The vessels were filled with hydrogen at room temperature and afterwards heated to the desired setpoint temperature. In order to perform absorption on several samples under the same conditions, steel inserts were used to fill the reactor simultaneously with different samples without the risk of cross-contamination.

Combined calorimetric and volumetric measurements were conducted in a coupled setup consisting of a Sensys DSC from Setaram and a PCTPro-2000 from Setaram & Hy-Energy. The samples (roughly 50 mg each) were heated at 5 K/min from room temperature to 550 °C in hydrogen atmosphere with pressures between 1 bar and 50 bar.

In situ synchrotron radiation powder X-ray diffraction (SR-PXD) experiments were conducted at the synchrotron facilities PETRA III (beamline P02.1) at DESY, Hamburg, Germany and MAX II (beamline I711) at MAX-lab, Lund, Sweden. The wavelengths at PETRA III and MAX II were $\lambda \approx 0.21$ Å and $\lambda \approx 0.99$ Å, respectively. The experiments were performed in Debye-Scherrer geometry with a special *in situ* diffraction setup[42,43] that allows for sample temperature and gas pressure recording. For this purpose, the specimen was filled into a sapphire capillary (⌀ 1 mm) which was positioned directly in the X-ray beam. This capillary was mounted into the sample holder body with gas-tight connections. A thermocouple inserted into the capillary with its tip almost in contact with the sample allowed for accurate temperature measurements. A pressure transducer connected to the sample holder was employed to ensure proper evacuation prior to as well as steady hydrogen pressure in the course of each *in situ* experiment. In order to determine the wavelength and the instrumental broadening precisely, LaB_6 powder was

used. An electrical heating block positioned below the capillary and operated by a PID controller increased the sample temperature with a rate of 5 K/min to the respective maximum. Acquisition times of 15 s (PETRA III) or 20 s (MAX II) were chosen for each diffraction pattern. The obtained 2-dimensional images were carefully masked and radially integrated by means of the program FIT2D[44,45].

Ex situ powder X-ray diffraction (PXD) data was collected with a Bruker D8 Discover diffractometer equipped with a Cu K_α source (λ = 1.54184 Å) and a XXX area detector operating in Bragg-Brentano geometry. To prevent samples from oxidation, a sample holder with an argon-filled PMMA dome was employed during the measurements. X-rays scattered at this dome were causing the broad background peak at roughly q = 1.5 $Å^{-1}$ that is present in each diffractogram.

The program MAUD[46,47] was used to perform Rietveld refinements of *ex situ* and selected *in situ* diffraction data. Crystallographic Information Files (CIF) were selected from the ICSD catalogue.

Solid-state magic angle spinning (MAS) nuclear magnetic resonance (NMR) spectra of the ^{11}B nucleus were recorded using a Bruker Avance 400 MHz spectrometer with a wide-bore 9.4 T magnet employing a boron-free Bruker CP-MAS probe or a ??? (Turin). Chemical shifts of the spectral frequency (128.33 MHz) were externally referenced to $BF_3{\cdot}Et_2O$ and reported in parts per million (ppm). The samples were filled into 4 mm ZrO_2 rotors that were closed with Kel-F caps. These rotors were spun at 12 KHz to 14 KHz by applying dry nitrogen gas. The temperature was kept at 20 °C by a Bruker BCU unit. In order to assess molar ratios of samples comprising more than one boron containing compound, the areas of resonances and their corresponding side bands in the range from 1500 ppm to -1500 ppm were considered. For the sake of comparability all spectra presented in this work were normalised by setting the total area to 1.

Materials and sample preparation

CaH_2 (98 %), MgH_2 (98 %), MgB_2 (XX %), Ni (99.8%) and CaB_6 (99.5 %) were purchased from Alfa Aesar, $Ca(BH_4)_2$ (95 %) and $CaB_{12}H_{12}$ (XX %) from KatChem. Boron (99 %) was received from Sigma-Aldrich. Mg_2NiH_4, $MgNi_{2.5}B_2$ and $Ca_4Mg_3H_{14}$ are not commercially available and were synthesised in-house.

In order to produce Mg_2NiH_4[48–54], MgH_2 and Ni were mixed in a molar ratio of 2:1 and milled for 4 hours in the planetary mill with a ball-to-powder ratio of 5:1 and a rotation speed of 300 rpm using Al_2O_3 vials. Subsequently, the mixture was annealed at 400 °C under hydrogen pressure of 225 bar. This back pressure value was chosen arbitrarily to prevent any dehydrogenation reaction.

$MgNi_{2.5}B_2$[55–57] was synthesised from a mixture of MgB_2 and Ni that was pre-milled for 4 hours in the planetary mill in Al_2O_3 vials. Also in this case a ball-to-powder ratio of 5:1 and a rotation speed of 300 rpm were applied. The ratio of these two compounds was 1:2.5. Afterwards, the powder was annealed at 930 °C in argon atmosphere for 24 h.

$Ca_4Mg_3H_{14}$[58–60] was prepared from a 4:3 mixture of CaH_2 and MgH_2 that was milled in the SPEX mill for 100 min with a ball-to-powder ratio of 10:1 using stainless steel vials. Subsequently, the material was heated to 400 °C under a hydrogen atmosphere of 200 bar. As for the synthesis of Mg_2NiH_4, the rather high but arbitrary hydrogen back pressure value was selected exclusively to prevent dehydrogenation reactions because no additional hydrogen is necessary to form $Ca_4Mg_3H_{14}$ from the 4:3 mixture of CaH_2 and MgH_2.

All standard samples that were used for the experiments shown below were prepared in the SPEX mill using stainless steel vials and employing a ball-to-powder ratio of 10:1 and a milling time of 300 min. The molar ratios of the different samples are summarised in Tab. 1.

In order to enhance reaction kinetics by decreasing the material's mean particle size[61,62], a particular specimen of CaH_2 - $MgNi_{2.5}B_2$ - MgH_2 was prepared by a sequence of intense ball milling cycles. First of all, the three components CaH_2, $MgNi_{2.5}B_2$ and MgH_2 were milled individually for 48 h in the planetary mill at a rotation speed of 350 rpm using WC vials and a ball-to-powder ratio of 40:1. Afterwards, a stoichiometric mixture of the pre-milled compounds was filled into a stainless steel high pressure vial. Heptane was added in a fluid-to-powder mass ratio of 4:1 to avoid particle agglomeration upon milling[63,64]. The obtained suspension was milled for 72 h at 400 rpm with a ball-to-powder ratio of 20:1. Subsequently the powder was separated from the liquid with a filter and then dried under continuous vacuum at 70 °C for 18 h.

Tab. 1 List of all mixed samples investigated in this publication with their respective chemical composition.

composite	molar ratio
$Ca(BH_4)_2$ - Mg_2NiH_4	1 : 2.5
CaH_2 - $MgNi_{2.5}B_2$ - MgH_2	1 : 1 : 4
CaH_2 - $MgNi_{2.5}B_2$	2 : 1
$MgNi_{2.5}B_2$ - MgH_2	1 : 5
$Ca_4Mg_3H_{14}$ - $MgNi_{2.5}B_2$ - MgH_2	1 : 4 : 13
$Ca_4Mg_3H_{14}$ - $MgNi_{2.5}B_2$	1 : 1
Mg_2NiH_4 - $CaB_{12}H_{12}$	15 : 1
Mg_2NiH_4 - CaB_6	7.5 : 1
Mg_2NiH_4 - B	1.25 : 1

Results

Several aspects of the dehydrogenation and (re)hydrogenation reactions of the $Ca(BH_4)_2$-Mg_2NiH_4 composite and its dehydrogenated state are presented hereafter. In particular, the influence of the hydrogen back pressure on the dehydrogenation reaction path is evaluated as well as the reactivity of typical decomposition products of $Ca(BH_4)_2$ with Mg_2NiH_4. Furthermore, a set of samples was dehydrogenated at different temperatures and times in order to assess the impact of these two parameters on the desorbed state and on the reversibility of this system. Eventually, the (re)hydrogenation

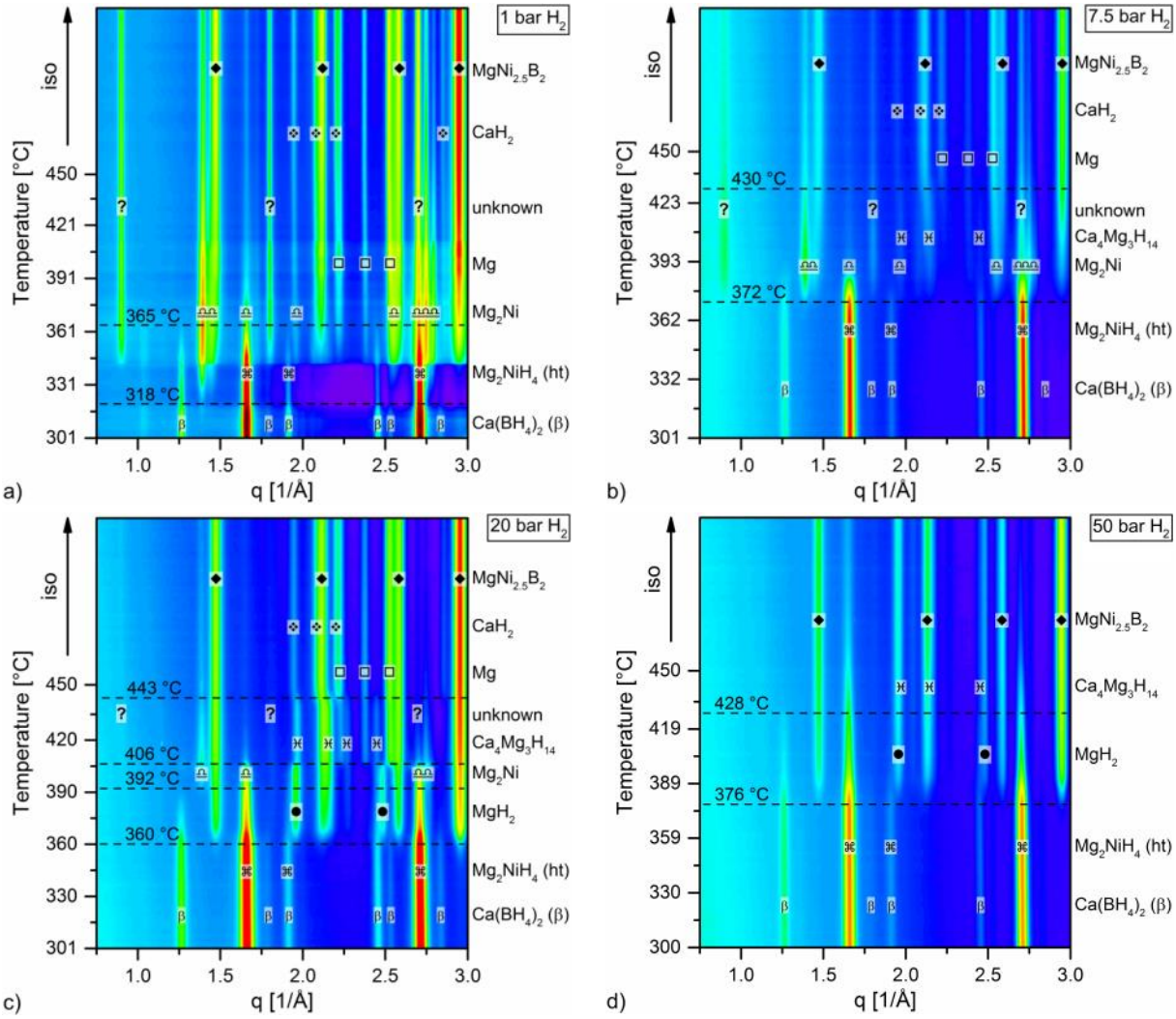

Fig. 1: In situ SR-PXD dehydrogenation experiments of $Ca(BH_4)_2$-Mg_2NiH_4 conducted at hydrogen pressures of 1 bar, 7.5 bar, 20 bar and 50 bar. The material was heated from room temperature to 450 °C at 5 K/min.

reactions were investigated and actions were taken to improve the absorption yield.

Influence of H_2 back pressure on dehydrogenation reactions

If reaction kinetics is sluggish it can be difficult to separate between thermodynamically controlled and kinetically hindered events, i. e. experimental techniques might not be able to resolve overlapping steps. In our previous communication[65] we presented an *in situ* SR-PXD experiment and the respective DSC analysis of the desorption of the $Ca(BH_4)_2$-Mg_2NiH_4 composite, both measured at 1 bar H_2. Basically all dehydrogenation reactions occurred at the same time leading to overlapping modifications of the diffraction patterns and a single, broad endothermic DSC peak. In order to shed some more light on those reactions, we repeated the measurements at pressures of 7.5 bar, 20 bar and 50 bar of hydrogen. The underlying idea is that all equilibrium temperatures of solid-gas reactions are shifted to higher values with increasing pressure. Kinetic constraints solely depend on the temperature, though. Therefore, at a certain pressure the equilibrium temperature of a particular reaction step is high enough to directly allow overcoming its activation energy. As a consequence, differences between thermodynamic equilibrium temperatures and measured dehydrogenation onsets (governed by kinetics) shrink with increasing hydrogen pressure and distinct reaction steps can be isolated on the temperature axis.

The evolution of crystalline phases upon dehydrogenation of the $Ca(BH_4)_2$-Mg_2NiH_4 sample was monitored by *in situ* SR-PXD experiments (Fig. 1). The sequences of diffraction patterns obtained under 1 bar, 7.5 bar, 20 bar and 50 bar H_2 are shown in a, b, c and d, respectively. As reported before[65], at temperatures below 300 °C only the polymorphous changes of $Ca(BH_4)_2$ and Mg_2NiH_4 can be observed. For this reason, the temperature axis of the presented results is narrowed down to the range 300 °C to 450 °C. Irrespective of the applied back pressure, the diffraction patterns taken at 300 °C exhibit exclusively the reflections of the high-temperature polymorphs β-$Ca(BH_4)_2$ ($P\bar{4}$)[66,67] and cubic Mg_2NiH_4 ($Fm\bar{3}m$)[49,50]. At 1 bar H_2 (Fig. 1 a), the dehydrogenation starts with the decomposition of Mg_2NiH_4 to Mg_2Ni and hydrogen at about 318 °C. The intensity of $Ca(BH_4)_2$

diffraction peaks begins to weaken soon after, while the reflections of four other phases occur and intensify, namely $MgNi_{2.5}B_2$, Mg, CaH_2 and an unknown phase. In the following, this unknown phase will be referred to as UP. At 365 °C the peaks of $Ca(BH_4)_2$ finally vanish. Simultaneously, the intensity of Mg_2Ni reflections maximises and quickly declines afterwards. The reflections of UP are intensifying up to roughly 410 °C and fading out subsequently. On the contrary, diffraction intensities of CaH_2, $MgNi_{2.5}B_2$ and Mg increase till the last diffractogram is taken. In the case of the dehydrogenation performed at 7.5 bar H_2 (Fig. 1 b), the sequence of events looks almost similar as compared to the experiment conducted at 1 bar H_2. The respective events are shifted to higher temperatures, though. Here, Mg_2NiH_4 starts to decompose at approximately 372 °C. However, there is one qualitative distinction, that is the initial formation of $Ca_4Mg_3H_{14}$ instead of CaH_2. At 430 °C also $Ca_4Mg_3H_{14}$ decomposes to CaH_2 and Mg. The dehydrogenation of $Ca(BH_4)_2$-Mg_2NiH_4 at 20 bar H_2 (Fig. 1 c) proceeds differently. As it can be seen, the very first modification in the diffraction patterns is the appearance of $Ca_4Mg_3H_{14}$, $MgNi_{2.5}B_2$ and MgH_2 at about 360 °C, accompanied by intensity reductions of $Ca(BH_4)_2$ and Mg_2NiH_4. At 392 °C the diffraction peaks of Mg_2Ni appear whereas those of Mg_2NiH_4 vanish completely. Additionally, rather weak peaks of UP can be recognised shortly after. MgH_2 decomposes at 406 °C and the reflections of Mg become visible. At 443 °C $Ca_4Mg_3H_{14}$ dehydrogenates to CaH_2 and Mg. Also in this experiment the intensities of Mg_2Ni and UP reduce gradually up to the last diffractogram. As with the experiment conducted at 20 bar, the very first event at a back pressure of 50 bar H_2 (Fig. 1 d) is the occurrence of reflections that can be attributed to $Ca_4Mg_3H_{14}$, $MgNi_{2.5}B_2$ and MgH_2 at roughly 376 °C. From this temperature on, the intensities of $Ca(BH_4)_2$ and Mg_2NiH_4 decrease. In contrast to the continuously fading out reflections of Mg_2NiH_4, the peaks of $Ca(BH_4)_2$ disappear abruptly at about 428 °C. Diffraction intensities of $Ca_4Mg_3H_{14}$, $MgNi_{2.5}B_2$ and MgH_2 increase till the last diffractogram. At this pressure, neither reflections of Mg_2Ni nor those belonging to UP can be perceived within the chosen temperature range.

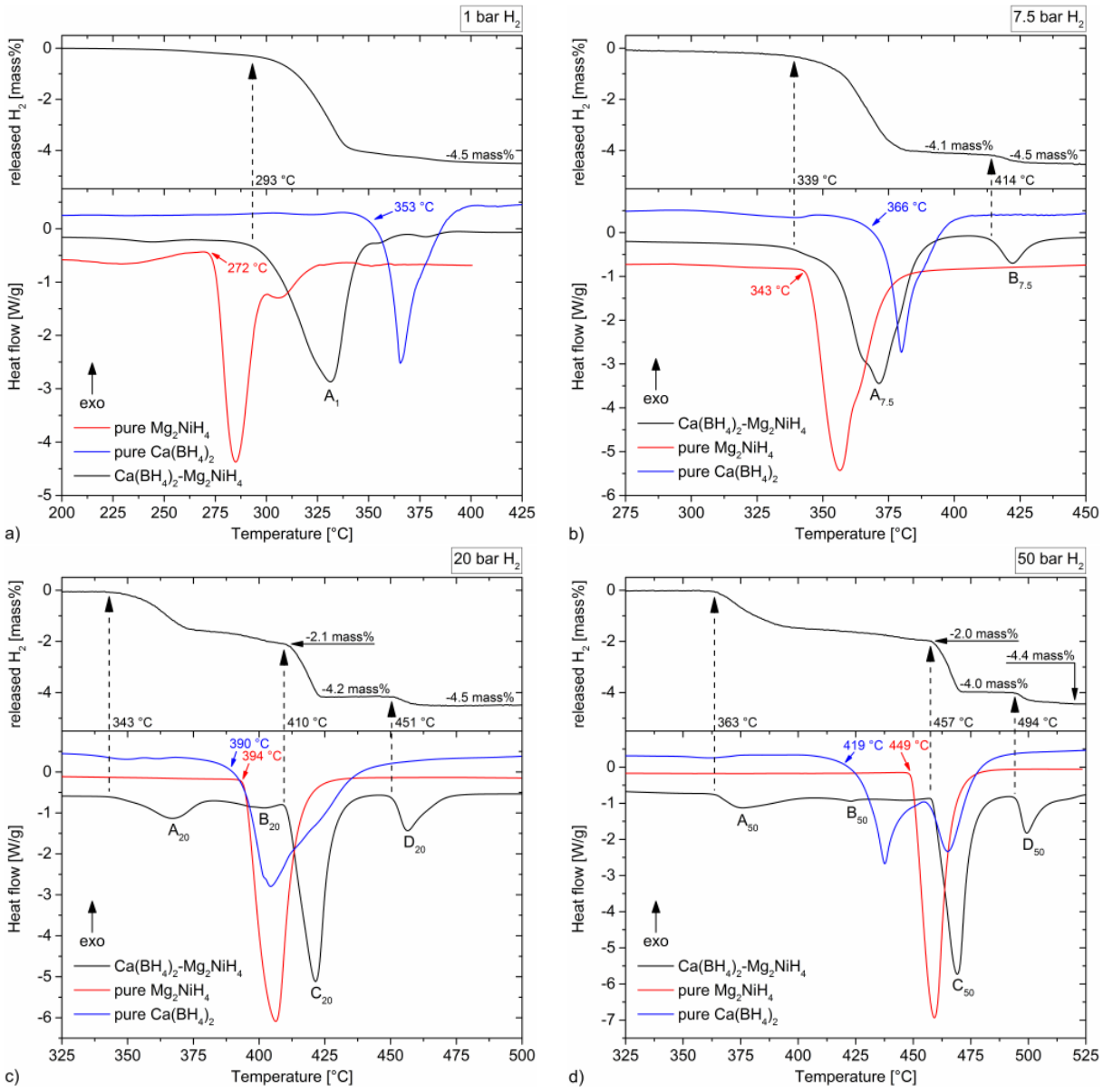

Fig. 2: Combined DSC and manometric analyses of $Ca(BH_4)_2$-Mg_2NiH_4, pure $Ca(BH_4)_2$ and pure Mg_2NiH_4. A hydrogen back pressure of 1 bar, 7.5 bar, 20 bar and 50 bar was applied, respectively. The materials were heated from room temperature to 550 °C at a rate of 5 K/min.

In order to correlate the crystallographic changes of $Ca(BH_4)_2$-Mg_2NiH_4 upon dehydrogenation to thermal transitions and the release of hydrogen, combined calorimetric and volumetric analyses were performed replicating the same experimental conditions as for the SR-PXD experiments (Fig. 2). For comparison, also the DSC curves of pure $Ca(BH_4)_2$ and Mg_2NiH_4 are included in this graph. These pure compounds were ball milled in exactly the same manner as all other samples to ensure comparable kinetic properties. Fig. 2 a shows the results of the desorptions conducted at 1 bar H_2. As described in our previous work[65], the composite $Ca(BH_4)_2$-Mg_2NiH_4 features one broad endothermic peak (A_1) with an onset temperature of 293 °C. This is 60 °C lower than the onset temperature of pure $Ca(BH_4)_2$ at 353 °C but 21 °C higher than the one of pure Mg_2NiH_4 at 272 °C. The material releases about 4.5 mass% H_2. At 7.5 bar H_2 (Fig. 2 b), the DSC trace of the hydride composite exhibits two separate endothermic peaks with onset temperatures of 339 °C ($A_{7.5}$) and 414 °C ($B_{7.5}$), respectively. Both peaks are related to the release of hydrogen. In the first event 4.1 mass% H_2 is evolved and additional 0.4 mass% H_2 in the second one. Hence, 4.5 mass% H_2 are desorbed in total. Compared to the pure compounds, the composite starts desorbing at about the same temperature as Mg_2NiH_4 (onset 343 °C) and 27 °C below that of $Ca(BH_4)_2$. The dehydrogenation experiments performed at a back pressure of 20 bar H_2 are presented in Fig. 2 c. As it can be seen, the DSC curve of the composite comprises four endothermic events. The onset temperatures of the peaks A_{20}, C_{20} and D_{20} are 343 °C, 410 °C and 451 °C, respectively. The second peak (B_{20}) is rather small, though. Its onset temperature cannot be determined clearly, also because this peak might be overlapping partially with A_{20}. Nevertheless, the onset of B_{20} is certainly below 390 °C. All four peaks are associated with the evolution of hydrogen. Approximately 2.1 mass% H_2 are released in the first two reaction steps (A_{20} and

B_{20}) and another 2.1 mass% H_2 in the reaction linked to C_{20}. In the last dehydrogenation step (D_{20}) 0.3 mass% H_2 evolves achieving an overall hydrogen loss of 4.5 mass%. Compared to pure $Ca(BH_4)_2$ and Mg_2NiH_4 (onsets at 390 °C and 394 °C), the temperature of the first dehydrogenation step of $Ca(BH_4)_2$-Mg_2NiH_4 (A_{20}) is reduced by about 50 °C. Fig. 2 d shows the analyses performed at 50 bar H_2. Similar to the results obtained at 20 bar, the DSC curve of the composite features four endothermic peaks (A_{50}, B_{50}, C_{50} and D_{50}). Due to its low intensity, the onset temperature of the second peak (B_{50}) is difficult to estimate, however, it seems to lay at around 420 °C. The other three onset temperatures are approximately at 363 °C (A_{50}), 457 °C (C_{50}) and 494 °C (D_{50}). Each thermal event is associated with hydrogen evolution. During the first two reaction steps (A_{50} and B_{50}) about 2.0 mass% H_2 are released. 2.0 mass% H_2 and 0.4 mass% H_2 are released in the third (C_{50}) and fourth (D_{50}) desorption step, respectively. Therefore, the total amount of desorbed hydrogen reaches 4.4 mass% H_2. The onset temperature of the first dehydrogenation step (A_{50}) is about 56 °C lower than the onset temperature of pure $Ca(BH_4)_2$ (419 °C) and 86 °C lower than the one of Mg_2NiH_4 (onset at 449 °C). By correlating the area of peak A_{50} with the amount of released hydrogen the reaction enthalpy of this desorption step can be estimated to approximately 15 kJ/(mol H_2).

If amorphous and/or nano-crystalline phases are involved in a chemical reaction, X-ray diffraction as well as calorimetric analyses do not provide sufficient information to fully elucidate the process. Thus, MAS NMR was employed to characterise the composition of desorbed samples with respect to ^{11}B-containing phases. For this purpose, three specimens of $Ca(BH_4)_2$-Mg_2NiH_4 were dehydrogenated at 50 bar H_2 and final temperatures of 370 °C, 400 °C and 450 °C for 20 h. The normalised NMR spectra are shown in Fig. 3. The chemical shifts of $Ca(BH_4)_2$ at -31 ppm[28,32], $CaB_{12}H_{12}$ at -15 ppm[37], boron at 0 ppm[28] and $MgNi_{2.5}B_2$ at 142 ppm[68] are emphasised. All the other signals visible in Fig. 3 are side bands of either $Ca(BH_4)_2$ or $MgNi_{2.5}B_2$. The spectrum of the sample desorbed at 370 °C features major resonance signals of $MgNi_{2.5}B_2$ and $Ca(BH_4)_2$. In addition, there is a very minor signal of $CaB_{12}H_{12}$. The sample heated to 400 °C contains less $Ca(BH_4)_2$ and more $MgNi_{2.5}B_2$ but also the fraction of $CaB_{12}H_{12}$ increased significantly. Furthermore, this sample seems to contain a small amount of boron. The sample heated up to 450 °C exhibits the highest degree of conversion to $MgNi_{2.5}B_2$ – the resonance of $Ca(BH_4)_2$ almost disappeared – but, as compared to the 400 °C sample, an even greater fraction of boron is bonded in $CaB_{12}H_{12}$ or the elemental state.

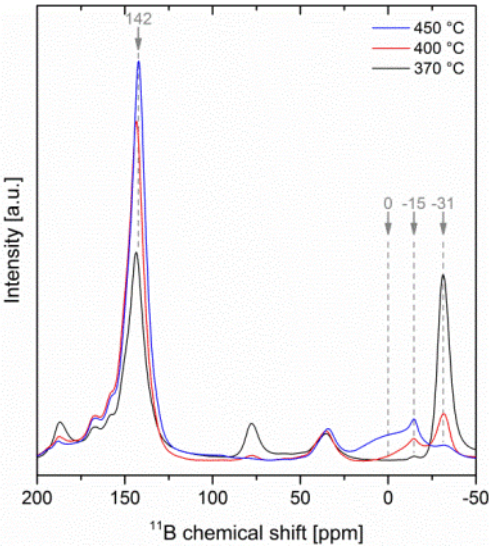

Fig. 4: Solid state ^{11}B MAS NMR spectra of samples of $Ca(BH_4)_2$-Mg_2NiH_4 dehydrogenated at 50 bar H_2 and temperatures of 370 °C, 400 °C and 450 °C, respectively.

Reactivity with decomposition products of $Ca(BH_4)_2$

By analysing the course of reflection intensities in the *in situ* SR-PXD experiments conducted at 1 bar, 7.5 bar and 20 bar H_2 (Fig. 1 a-c) one can observe that the peaks of Mg_2Ni fade out whilst those of $MgNi_{2.5}B_2$ intensify after the diffraction peaks of $Ca(BH_4)_2$ already vanished. Since an additional boron source is required to form $MgNi_{2.5}B_2$ from Mg_2Ni, it is reasonable to consider non-diffractive decomposition products of $Ca(BH_4)_2$ as potential boron donors. In order to investigate this possibility, the three most common boron containing decomposition products of $Ca(BH_4)_2$, namely $CaB_{12}H_{12}$, CaB_6 and elemental boron, were chosen for an investigation of their reactivity with Mg_2NiH_4.

Mixtures of Mg_2NiH_4 with $CaB_{12}H_{12}$, CaB_6 and elemental boron were prepared in molar ratios of 15:1, 7.5:1 and 1.25:1, respectively, in order to meet the atomic ratio of Ni and boron in $MgNi_{2.5}B_2$. Samples of these three mixtures were heated to 450 °C in 1 bar H_2 and kept isothermally for 20 h. Afterwards PXD measurements were conducted on the obtained materials (Fig. 4). All diffraction patterns clearly show the reflections of $MgNi_{2.5}B_2$ and Mg. In case of the samples initially prepared with $CaB_{12}H_{12}$ and CaB_6, no diffraction peaks of other

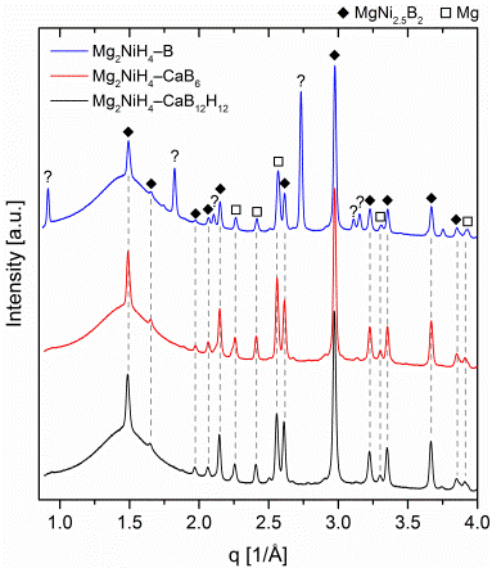

Fig. 3: PXD analyses of the reactions products between Mg_2NiH_4 and $CaB_{12}H_{12}$, CaB_6 or boron. All samples were heated to 450 °C at a hydrogen pressure of 1 bar.

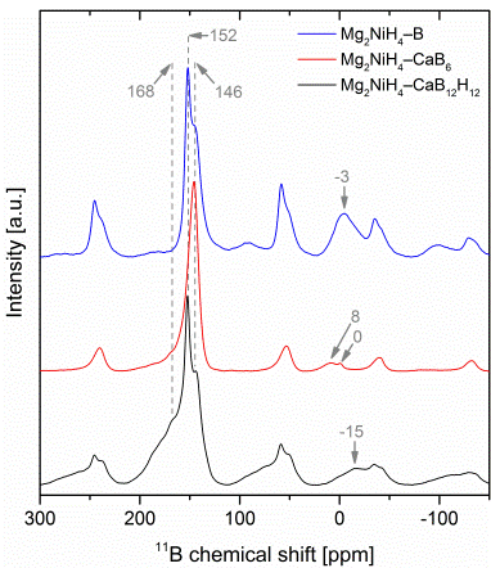

Fig. 5: ^{11}B MAS NMR spectra of the reaction products between Mg_2NiH_4 and $CaB_{12}H_{12}$, CaB_6 or boron. All samples were heated to 450 °C at a hydrogen pressure of 1 bar.

compounds can be clearly recognised. Rietveld analyses of the two diffraction patterns suggest the presence of CaH_2, though. The low intensity reflections are covered by peaks of $MgNi_{2.5}B_2$. In contrast, the diffractogram of dehydrogenated Mg_2NiH_4-B additionally displays the reflections of UP.

Solis state ^{11}B MAS NMR analyses of the same samples are presented in Fig. 5 and show to what extent boron is transferred to $MgNi_{2.5}B_2$ upon heat treatment. The resonances of $MgNi_{2.5}B_2$ (≈ 170 ppm to 140 ppm), $CaB_{12}H_{12}$ (-15 ppm), CaB_6 (≈ 8 ppm and 0 ppm) and boron (≈ 3 ppm) are marked. In all three samples most of the boron is bonded in $MgNi_{2.5}B_2$. In case of dehydrogenated Mg_2NiH_4-$CaB_{12}H_{12}$, $MgNi_{2.5}B_2$ contains about 96 % of all boron atoms; the rest is bonded in residual $CaB_{12}H_{12}$. Hence, the molar ratio of $MgNi_{2.5}B_2$ and $CaB_{12}H_{12}$ is roughly 144:1. For reacted Mg_2NiH_4-CaB_6 approximately 97 % of the boron atoms were transferred to $MgNi_{2.5}B_2$ which is equivalent to a molar ratio of about 97:1 for $MgNi_{2.5}B_2$ and CaB_6. The heated specimen of Mg_2NiH_4-B possesses the highest fraction of initial reactants; about 28 % of boron is still present in the elemental state. This corresponds to a molar ratio of $MgNi_{2.5}B_2$ and B of approximately 1.3:1.

SR-PXD measurements showing the reaction paths of Mg_2NiH_4-$CaB_{12}H_{12}$ and Mg_2NiH_4-CaB_6 are presented in Fig. 6. Reaction kinetics of Mg_2NiH_4-B was too sluggish to allow for the observation by *in situ* diffraction analysis in a reasonable time frame. The specimens of the two other composites were heated to 450 °C in 1 bar H_2. Since $CaB_{12}H_{12}$ is typically non-diffractive, only peaks of Mg_2NiH_4 can be identified in Fig. 6 a up to 319 °C. At this temperature, Mg_2NiH_4 decomposes and the reflections of Mg_2Ni arise. At about 383 °C $MgNi_{2.5}B_2$ and UP are formed simultaneously. Their peaks intensify till the termination of the experiment. Also in case of Mg_2NiH_4-CaB_6 the decomposition of Mg_2NiH_4 occurs at 319 °C but unlike the priorly discussed experiment the emerging reflections of Mg_2Ni remain the only new peaks during the heating period. Nevertheless, after a short incubation time at 450 °C the peaks of $MgNi_{2.5}B_2$ and UP arise at more or less the same time. Possibly the growth of UP crystallites is slightly faster in this initial stage.

Influence of desorption time and temperature on the dehydrogenated state and the reversibility of the system

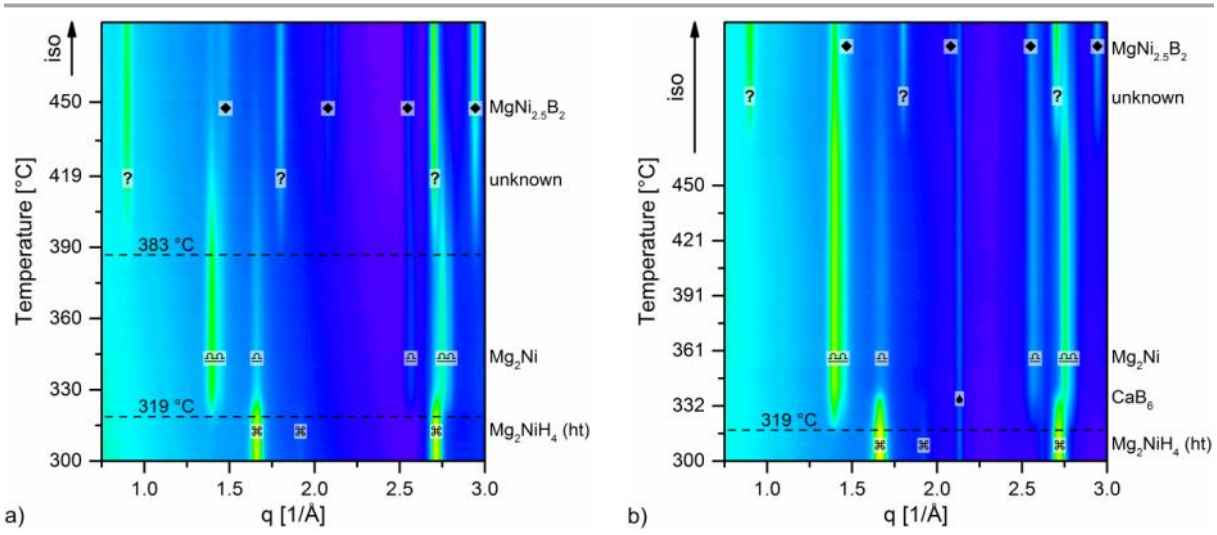

Fig. 6: In situ SR-PXD experiments of Mg_2NiH_4-$CaB_{12}H_{12}$ (a) and Mg_2NiH_4-CaB_6 (b): the specimens were heated in a hydrogen atmosphere of 1 bar from room temperature to 450 °C at 5 K/min.

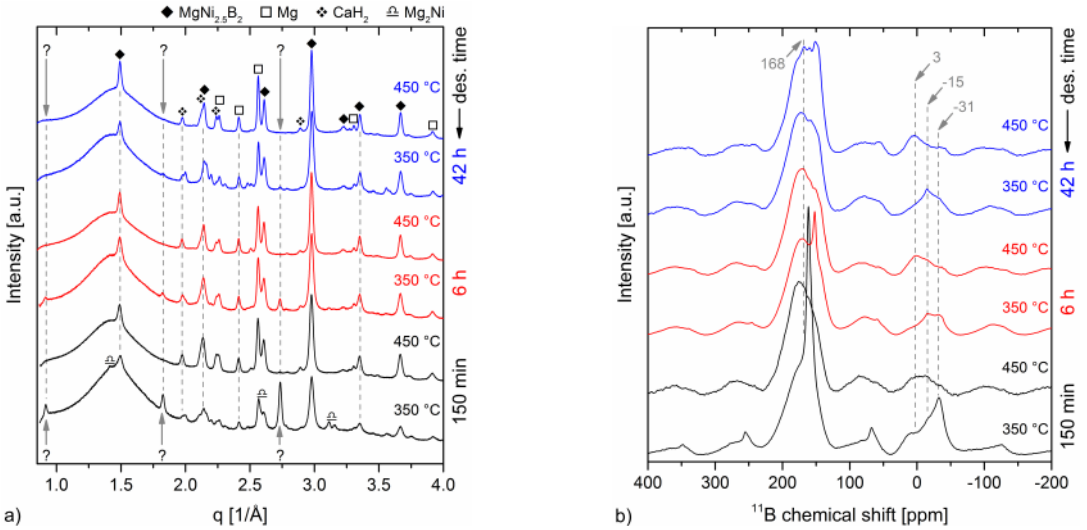

Fig. 7: PXD analyses (a) and ^{11}B MAS NMR spectra (b) of the dehydrogenation product of $Ca(BH_4)_2$-Mg_2NiH_4: all samples were heated to their respective maximum temperatures (350 °C, 400 °C or 450 °C) in 1 bar H_2, the dwell time was varied in order to establish equal total desorption times (150 min, 6 h or 42 h) for samples of the same set (same colour).

In general, the temperature and duration chosen for dehydrogenation potentially influence the reaction path as well as the degree of conversion and thus the composition and microstructure of the desorbed state. Furthermore, intermediate phases can be metastable at lower temperatures. On the contrary, longer annealing times and higher temperatures result in larger crystallite and grain sizes of the desorption products in addition to a reduction of the number of crystallographic defects. Hence, changes in the related activation energies might also affect the reabsorption reactions and therefore the degree of reversibility. In order to characterise these influences on $Ca(BH_4)_2$-Mg_2NiH_4, a set of samples was desorbed at 350 °C and 450 °C, respectively, with increasing desorption times and reabsorbed afterwards.

In total six samples were dehydrogenated at a pressure of 1 bar H_2 and then characterised by *ex situ* PXD and NMR analyses. Fig. 7 a shows the diffraction patterns of these samples, the related ^{11}B NMR spectra are presented in Fig. 7 b. All samples were heated to their respective maximum temperatures at the same rate but the subsequent isothermal dwell time was varied. Charts with the same colour represent samples with equal total desorption time, i. e. the isothermal time was altered in such a manner that the overall time of both, heating period and dwell time, was equal for desorptions of the same set. Charts of samples with a total desorption time of 150 minutes are shown in black. Red and blue charts indicate total desorption times of 6 and 42 hours, respectively. All diffractograms presented in Fig. 7 a exhibit the reflections of $MgNi_{2.5}B_2$, Mg and CaH_2. The samples dehydrogenated at 350 °C additionally feature the diffraction peaks of UP. The highest intensity of these reflections can be perceived in the diffractogram of the sample with a total dehydrogenation time of 150 min. By increasing the isothermal heating period the respective peak intensities first decline (6 h) and eventually almost vanish (42 h). Traces of Mg_2Ni can only be recognised in case of the sample desorbed at 350 °C for 150 min. As can be seen in Fig. 7 b, in all samples by far the largest fraction of boron is bonded in $MgNi_{2.5}B_2$. In all spectra, the resonance of this compound is very broad and exhibits a rather asymmetric shape; the particular centre band positions are all at about 168 ppm. The resonances of $Ca(BH_4)_2$ (-31 ppm), $CaB_{12}H_{12}$ (-15 ppm), CaB_6 (0 and 8 ppm) and elemental boron (-3 ppm) are all overlapping with the second side band of $MgNi_{2.5}B_2$ on the right hand side. In conjunction with the irregular shapes of the $MgNi_{2.5}B_2$ peak in these spectra, it is hard to separate contributions of individual compounds if those are present just in small quantities. Some assumptions can be made, though. Focussing first on the samples heated to 350 °C, the one dehydrogenated for only 150 min clearly contains residual $Ca(BH_4)_2$, minor amounts of $CaB_{12}H_{12}$ and presumably traces of boron or CaB_6. The sample desorbed for 6 h also shows weak signals that can be attributed to $CaB_{12}H_{12}$ and $Ca(BH_4)_2$; the amount of $Ca(BH_4)_2$ is yet much less than in the sample with the short dehydrogenation time. After 42 h at 350 °C no more

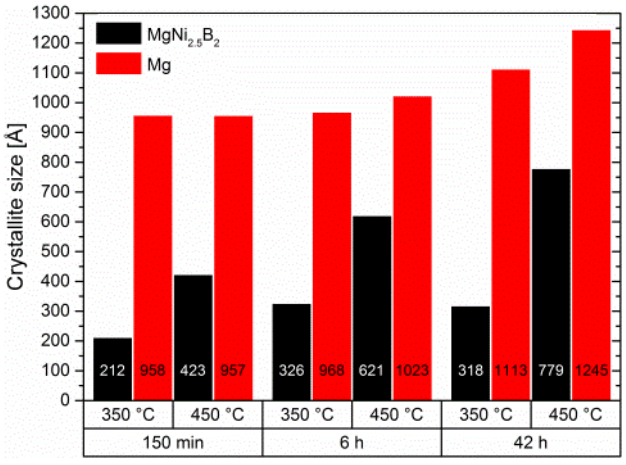

Fig. 8: Determined mean sizes of $MgNi_{2.5}B_2$ and Mg crystallites for all samples shown in Fig. 7.

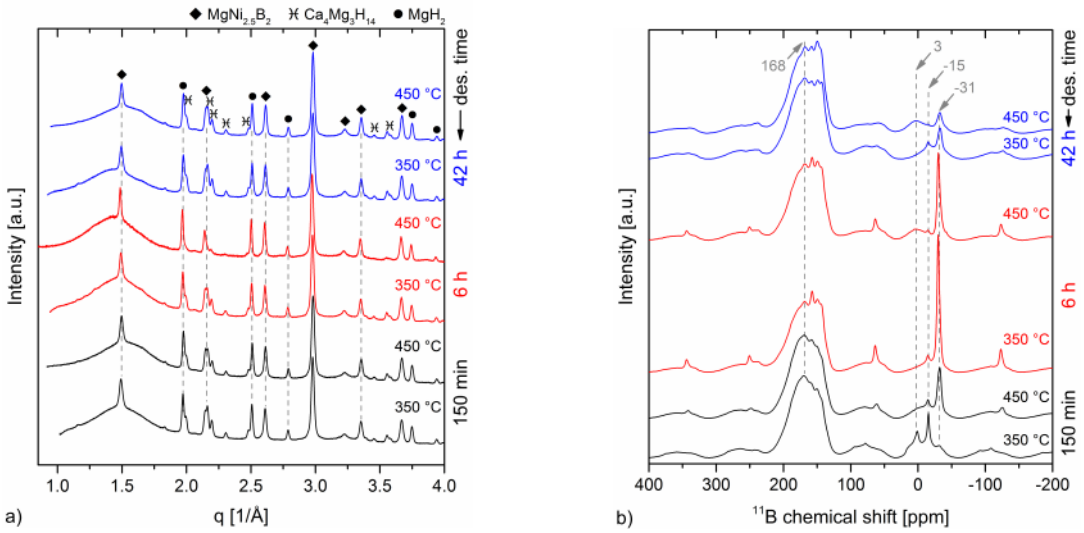

Fig. 9: PXD analyses (a) and ^{11}B MAS NMR spectra (b) of the $Ca(BH4)_2$-Mg_2NiH_4 samples desorbed at different temperatures and for different durations (see Fig. 7) after rehydrogenation.

$Ca(BH_4)_2$ is discernible but only a small fraction of $CaB_{12}H_{12}$. In contrast, by heating $Ca(BH_4)_2$-Mg_2NiH_4 to 450 °C, all $Ca(BH_4)_2$ decomposes in the first 150 min. However, weak signals of what could be CaB_6 and/or elemental boron can be noticed also after 42 h. Mean crystallite sizes of $MgNi_{2.5}B_2$ and Mg in the desorbed samples were evaluated as part of the Rietveld analyses and are presented in Fig. 8. As expected from the respective melting temperatures, in all investigated samples the crystallites of $MgNi_{2.5}B_2$ are significantly smaller than those of Mg. The influence of the dehydrogenation time and temperature on the crystallite growth of the two compounds is apparent as, for instance, $MgNi_{2.5}B_2$ crystallites are approximately doubled in size if the desorption temperature is increased from 350 °C to 450 °C.

In order to investigate the influence of the desorption temperature and time on the reversibility of this hydride composite, the samples were rehydrogenated. For sake of comparability, the hydrogenation of all six samples was performed simultaneously in the same autoclave. After charging with 250 bar H_2 at room temperature, this autoclave was heated to 400 °C within 80 min and subsequently kept at this temperature for 16 h. Diffractograms and ^{11}B NMR spectra of the rehydrogenated powders are presented in Fig. 9. All samples contain $MgNi_{2.5}B_2$, $Ca_4Mg_3H_{14}$ and MgH_2. These are the only diffractive phases present in larger quantities (Fig. 9 a). The specimen previously dehydrogenated at 350 °C for 6 h features two small peaks at 1.21 Å^{-1} and 1.28 Å^{-1} that could be assigned to the (111) reflection of α- ($F2dd$)[67] and the (110) reflection of β-$Ca(BH_4)_2$ ($P\bar{4}$)[67]. However, the intensities of these peaks are very low and all other potential reflections of the two $Ca(BH_4)_2$ polymorphs are possibly overlapping with other diffractions peaks. Therefore, the presence of $Ca(BH_4)_2$ in this sample cannot be confirmed with a sufficient degree of accuracy and reliability by a Rietveld refinement of the X-ray diffractogram. At this point the ^{11}B NMR analyses provide clear evidence that $Ca(BH_4)_2$ is actually present not only in this particular sample but in all samples. However, the rehydrogenated sample that was initially desorbed at 350 °C for 6 h apparently contains the highest fraction of $Ca(BH_4)_2$ among all the presented samples. Although the $Ca(BH_4)_2$ resonance exhibits the highest intensity of all peaks in this spectrum, the molar ratio of $Ca(BH_4)_2$ and $MgNi_{2.5}B_2$ is only about 0.25. Considering the amount of formed $Ca(BH_4)_2$ as a measure for the degree of reversibility, a value of roughly 20 % was reached. At approximately 14 % of all boron bonded in $Ca(BH_4)_2$, the sample previously desorbed at 450 °C for 6 h shows the second highest degree of reversibility. All other samples feature reversibility levels of well below 10 %. In addition, small quantities of $CaB_{12}H_{12}$ can be perceived in all samples. The highest amount is found in the sample initially desorbed at 350 °C for 150 min. This sample, as well as all the samples dehydrogenated at 450 °C, additionally seem to contain traces of elemental boron and/or CaB_6.

Analysing the absorption process by hydrogenation of different as-prepared desorbed state samples

In order to obtain deeper insights into the absorption processes and potential constraints, the role and importance of the different components in the fully desorbed state had to be examined. As described earlier, these components are CaH_2, $MgNi_{2.5}B_2$ and Mg. The possibility to hydrogenate specimen without either CaH_2 or Mg should be investigated. Moreover, upon hydrogenation of desorbed $Ca(BH_4)_2$-Mg_2NiH_2, a partially hydrogenated state is created first as MgH_2 is formed. Subsequently, CaH_2 is gradually consumed due to the formation of $Ca_4Mg_3H_{14}$. This reaction proceeds without absorption of gaseous hydrogen. Hence, the partially hydrogenated state is modified but the degree of hydrogenation remains unchanged. However, at the chosen absorption conditions, the formation of the ternary hydride reduces the Gibbs free energy of the partially hydrogenated state[29]. Therefore, the Gibbs free energy change is reduced for the formation of $Ca(BH_4)_2$ from the $Ca_4Mg_3H_{14}$ based intermediate state with respect to the corresponding state comprising "$4CaH_2 + 3MgH_2$". As a consequence, the formation of $Ca_4Mg_3H_{14}$ in the absorption process is expected to increase the sorption equilibrium pressure. In

addition, the evolution of this compound might also change kinetic barriers. A similar reaction behaviour could be observed in the system CaH_2-MgB_2: if absorption temperature and pressure are not high enough, the side reaction forming $Ca_4Mg_3H_{14}$ would stop further formation of $Ca(BH_4)_2$[69–71].

Five samples with different compositions were prepared by ball milling. These are CaH_2-$MgNi_{2.5}B_2$-MgH_2, CaH_2-$MgNi_{2.5}B_2$, $MgNi_{2.5}B_2$-MgH_2, $Ca_4Mg_3H_{14}$-$MgNi_{2.5}B_2$-MgH_2 and $Ca_4Mg_3H_{14}$-$MgNi_{2.5}B_2$. The molar ratios are summarised in Tab. 1. Due to the ductility of elemental Mg and the resulting cold-welding phenomena under ball milling, MgH_2 was used instead. Hereby, the absorption properties remain unimpaired because, due to the fast hydrogenation kinetics of Mg, the formation of MgH_2 is the first reaction step anyway. The five samples were absorbed at the same time in the autoclave. For that purpose the vessel was charged with 230 bar H_2 at room temperature and heated to 400 °C within 80 min. A final pressure of 410 bar was reached and kept for 48 h. ^{11}B NMR analyses of the hydrogenated samples are presented in Fig. 10. All samples show the resonance of unreacted $MgNi_{2.5}B_2$ at 141 ppm. The CaH_2-$MgNi_{2.5}B_2$-MgH_2 sample that corresponds to the actual composition of the dehydrogenation products of $Ca(BH_4)_2$-Mg_2NiH_2 additionally features a weak signal of $Ca(BH_4)_2$ at -31 ppm. The two samples without either CaH_2 or MgH_2 do not show any signals besides $MgNi_{2.5}B_2$. In contrast, hydrogenation of $Ca_4Mg_3H_{14}$-$MgNi_{2.5}B_2$-MgH_2 led to the highest degree of $Ca(BH_4)_2$ formation as can be seen at the strong intensity of its resonance peak. An additional resonance at -41 ppm can be recognised. This signal can be attributed to $Mg(BH_4)_2$.[72,73] Also absorbed $Ca_4Mg_3H_{14}$-$MgNi_{2.5}B_2$ exhibits the signals of the two different borohydrides, the intensities are yet much lower than in the case with MgH_2 addition. The two samples with $Ca_4Mg_3H_{14}$ as an initial reactant show the highest absorption yields among the five samples that are presented here.

Optimising the hydrogenation yield

The results of the last section suggest that the rather low absorption yields that were achieved in most hydrogenation attempts must be attributed to sluggish reaction kinetics due to poor solid state diffusion rates. A common way to address such kinetic limitations is the reduction of particle sizes[61,62]. This leads to shorter diffusion lengths and larger contact areas of the different reactants. The preparation of special desorbed state material with a low mean particle size is described in detail in the experimental section. This material is referred to as BMH (for ball milled in heptane).

The as-milled material (approx. 7 g) was hydrogenated in the autoclave that was charged with 250 bar H_2 at room temperature, heated to 400 °C within 80 min and kept isothermally for 15 h. At the end of the hydrogenation period and before cooling down a pressure of 310 bar was measured. A specimen of the absorbed material was kept as a reference (BMH, 1. abs. step). One part of the remaining material was milled in the Spex mill for 100 min and filled into the autoclave afterwards. Without additional treatment, the rest of the powder was separately filled into the autoclave, too. The second absorption step was performed in the exact same manner as the first step (final pressure 420 bar). Afterwards, the material that was milled after the first absorption step was milled further for 100 min and returned to the autoclave. A third hydrogenation step was conducted similarly to the previous steps (final pressure 420 bar). Subsequently, specimens were taken from both the material with the intermediate milling cycles (BMH, 3. abs. step, intermediate milling) and the material that was simply absorbed in three steps without additional treatment (BMH, 3. abs. step, w/o intermediate milling). For comparison an additional specimen of as-milled BMH was absorbed (2. BMH, 1. abs. step). In

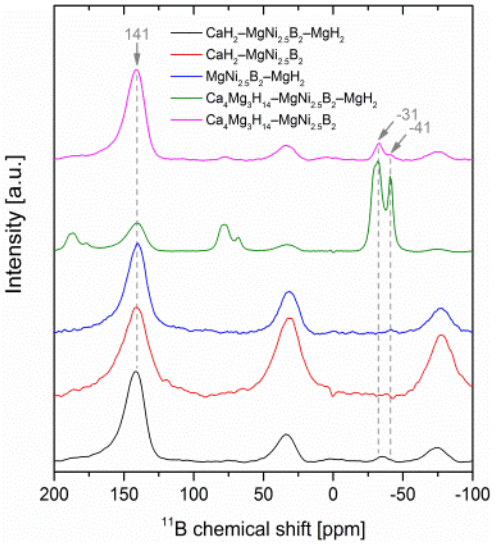

Fig. 11: ^{11}B NMR analyses after hydrogenation of different as-prepared desorbed state samples.

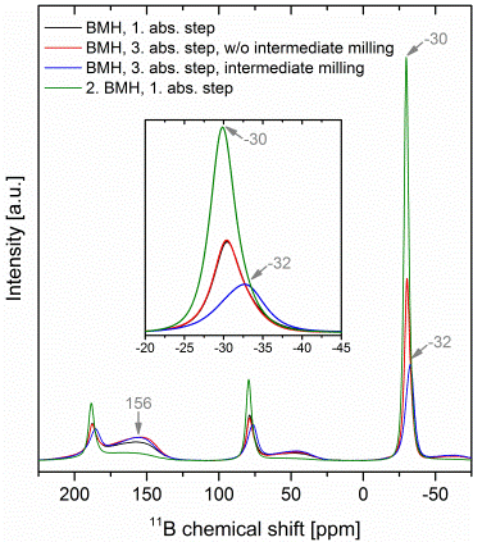

Fig. 10: ^{11}B NMR spectra of hydrogenated samples of CaH_2 - $MgNi_{2.5}B_2$ - MgH_2 (low mean particle size due to intense ball milling in heptane). The numbers in the caption confuses the reader in my opinion, especially the points in place of th and the last line.

contrast to the previous three absorption iterations, this time only 200 mg of material were used and the autoclave was charged with an initial H_2 pressure of 270 bar. As a consequence, the final hydrogen pressure before cooling down was 440 bar.

^{11}B NMR spectra of the two different samples after one absorption step and of the two samples after three absorption steps are presented in Fig. 11. Due to the normalisation of total areas, the different spectra are directly comparable. After the first absorption step (BMH, 1st abs. step), an absorption yield of approximately 63 % was reached. Without the application of intermediate milling cycles the two additional absorption iterations did not lead to an improved absorption yield. The corresponding spectrum (BMH, 3rd abs. step, w/o intermediate milling) looks almost identical to the one after the first absorption. In contrast, after three absorption steps with intermediate milling cycles (BMH, 3rd abs. step, intermediate milling) the intensity of the $Ca(BH_4)_2$ resonance dropped and the peak maximum shifted from -30 ppm to -32 ppm. However, the total area related to the $Ca(BH_4)_2$ signal (main peak incl. side bands) remained unchanged because the width of the resonance peak as well as the relative intensities of the side bands increased. Thus, also after three absorption steps with intermediate milling cycles the absorption yield did not improve and remained 63 %. The sample of as-milled BMH hydrogenated at higher hydrogen pressure led to improved conversion of the starting reactants. An absorption yield of 87 % was reached.

Discussion

The experiments conducted with varying hydrogen pressure clearly confirm the strong influence of the pressure on the dehydrogenation path of $Ca(BH_4)_2$-Mg_2NiH_4. At 1 bar H_2 several reaction steps overlap (Fig. 1 a and Fig. 2 a). At this pressure, the initial event is the desorption of Mg_2NiH_4. Immediately afterwards, the newly formed alloy Mg_2Ni reacts with $Ca(BH_4)_2$ to $MgNi_{2.5}B_2$, CaH_2, Mg and UP. The broad DSC peak A_1 embraces all these overlapping reactions. As we reported earlier, UP is an intermediate compound that degrades slowly. Also at 7.5 bar H_2, the first reaction step is still the independent dehydrogenation of Mg_2NiH_4 but the follow-up reactions are slightly altered as compared to the desorption at 1 bar. The increased pressure enables the formation of $Ca_4Mg_3H_{14}$ – a ternary hydride that is more stable than MgH_2[59] – besides $MgNi_{2.5}B_2$, Mg and UP. The DSC peak $A_{7.5}$ in Fig. 2 b comprises these reactions. The second peak in this figure ($B_{7.5}$) is associated to the decomposition of $Ca_4Mg_3H_{14}$. The dehydrogenation of $Ca(BH_4)_2$-Mg_2NiH_4 conducted at 20 bar H_2 shows one significant difference in comparison to those performed at lower pressures: the first reaction step – the formation of $MgNi_{2.5}B_2$, $Ca_4Mg_3H_{14}$ and MgH_2 (Fig. 1 c at 360 °C, Fig. 2 c peak A_{20}) – occurs prior to the desorptions of residual Mg_2NiH_4 and $Ca(BH_4)_2$ (Fig. 1 c at 392 °C, Fig. 2 c peak B_{20}). This result suggests that the two complex hydrides, $Ca(BH_4)_2$ and Mg_2NiH_4, actually destabilise each other and react directly without initial dehydrogenation of the less stable hydride. By comparing the DSC analysis with the related *in situ* SR-PXD experiment, the DSC peaks C_{20} and D_{20} can be assigned to the desorptions of MgH_2 and $Ca_4Mg_3H_{14}$, respectively. Furthermore, weak reflections of UP appear in conjunction with those of Mg_2Ni once the decomposition temperature of Mg_2NiH_4 is exceeded (Fig. 1 c at 392 °C). This observation implies that the reaction path leading to UP requires Mg_2Ni as reactant. Similarly to the experiment performed at 20 bar H_2, the first reaction step observed at 50 bar is the formation of $MgNi_{2.5}B_2$, $Ca_4Mg_3H_{14}$ and MgH_2 (Fig. 1 d at 376 °C, Fig. 2 d peak A_{50}) without the direct decomposition of Mg_2NiH_4. Due to the hydrogen back pressure of 50 bar, the equilibrium temperature of Mg_2NiH_4 was not exceeded in the course of the entire SR-PXD experiment (max. temperature limited to 450 °C) and consequently no Mg_2Ni was formed. There are also no reflections of UP discernible throughout the whole experiment which suggests once more that Mg_2Ni is an essential reactant for the formation of UP. In contrast to Mg_2NiH_4, residual $Ca(BH_4)_2$ does decompose independently as can be seen from the disappearance of its diffraction peaks at about 428 °C in Fig. 1 d and the small DSC peak B_{50} in Fig. 2 d. The last two DSC events in Fig. 2 d, C_{50} and D_{50}, are related to the desorption of MgH_2 and $Ca_4Mg_3H_{14}$, respectively. As just pointed out, at higher hydrogen pressures (here at 20 bar and 50 bar) the first dehydrogenation step seems to be a concerted reaction between $Ca(BH_4)_2$ and Mg_2NiH_4. This conclusion appears reasonable because the onset temperature of this reaction is lower than the decomposition temperatures of the pure compounds. Additionally, no reflections of Mg_2Ni are discernible in the corresponding SR-PXD experiments. However, decomposition products of $Ca(BH_4)_2$ tend to be non-diffractive[27,28,32,34,35]. Thus, the possibility is given that a partial or gradual desorption of $Ca(BH_4)_2$ into any of these non-diffractive phases initialises the first, presumably concerted, reaction step. A rather conclusive argument that also $Ca(BH_4)_2$ does not desorb independently prior to the reaction forming $MgNi_{2.5}B_2$ is provided by the ^{11}B NMR analyses of the specimens desorbed at 50 bar H_2 and temperatures of 370 °C, 400 °C and 450 °C. The presence of residual $Ca(BH_4)_2$ in all samples shows that none of them dehydrogenated completely. Consequently, the spectra provide insights into an intermediate dehydrogenation state. At all temperatures the transfer of boron to $MgNi_{2.5}B_2$ proceeds with the fastest reaction rate since this compound constitutes the highest molar fraction among all boron containing phases. Although a very small fraction of $CaB_{12}H_{12}$ is discernible already at 370 °C, indicating that $Ca(BH_4)_2$ decomposed partially by itself, the peaks of $CaB_{12}H_{12}$ and elemental boron are much more pronounced at 400 °C and 450 °C. Therefore, by lowering the temperature below 370 °C the decomposition of $Ca(BH_4)_2$ can be suppressed without restraining the reaction path forming $MgNi_{2.5}B_2$. This finding is in accordance with the DSC and SR-PXD results and supports the assumption of a concerted reaction between $Ca(BH_4)_2$ and Mg_2NiH_4 at back pressures of hydrogen higher than (at least) 7.5 bar. In this regard, the possibility of a concerted reaction between $LiBH_4$ and Mg_2NiH_4 was discussed previously by Vajo et al.[74] They investigated a 2:2.5-mixture of those two complex hydrides and presented desorption curves of this composite in comparison to the pure compounds, showing that the dehydrogenation of the composite started well below those of pure $LiBH_4$ and Mg_2NiH_4. The authors claimed that this was the first reported reversible composite consisting of at least two hydrides that shows such a behaviour i. e. the mutual destabilisation of both

hydrides. To the best of our knowledge, $Ca(BH_4)_2$-Mg_2NiH_4 is the second borohydride-based composite studied that exhibits this characteristic. It is likely that Mg_2NiH_4 enables the concerted reactions in these composite systems. As suggested by Vajo et al., the complex anion $[NiH_4]^{4-}$ might have some catalytic activity due to the Ni core.

Considering only those crystalline compounds that could be detected in the SR-PXD experiments, hence neglecting the possible presence of small quantities of amorphous and/or nano-crystalline phases (i. e. CaB_xH_y, boron), the release of hydrogen can be attributed to the following three thermodynamic reaction steps:

$$Ca(BH_4)_2 + 2.5Mg_2NiH_4 \rightarrow 0.25Ca_4Mg_3H_{14} + MgNi_{2.5}B_2 + 3.25MgH_2 + \underbrace{4H_2}_{2.3\ mass\%} \quad (1)$$

$$\rightarrow 0.25Ca_4Mg_3H_{14} + MgNi_{2.5}B_2 + 3.25Mg + \underbrace{7.25H_2}_{4.2\ mass\%} \quad (2)$$

$$\rightarrow CaH_2 + MgNi_{2.5}B_2 + 4Mg + \underbrace{8H_2}_{4.6\ mass\%} . \quad (3)$$

The reactions do not include Mg_2Ni and UP because these two phases do not exist in thermodynamic equilibrium but must be considered as intermediates. The theoretical amounts of hydrogen that evolve in each step are expressed in mass% with respect to the initial mass of the composite. At a pressure of 1 bar H_2, the material desorbs directly according to reaction 3 involving Mg_2Ni and UP as intermediate phases. By increasing the pressure to 7.5 bar, two dehydrogenation steps could be observed, namely the reactions 2 – again containing Mg_2Ni and UP temporarily – and 3. At 20 bar and 50 bar, the dehydrogenation proceeds *via* all three steps where reaction 1 constitutes the concerted reaction. For all investigated pressures the determined quantities of hydrogen that are released in the particular steps (Fig. 2 a-d) are in good agreement with the theoretical values. This fact already indicates that no or just minor fractions of non-diffractive, hydrogen containing side products were formed upon desorption.

It is noteworthy that at 15 kJ/(mol H_2) the estimated enthalpy change of reaction 1 is relatively low. Compared to thermodynamic data obtained from pressure-composition isotherms, enthalpy values collected from DSC analyses are typically less accurate, especially if the investigated reaction proceeds with sluggish kinetics. However, the measured value still provides the correct magnitude. Moreover, for the $LiBH_4$-Mg_2NiH_4 system a similarly low reaction enthalpy (15.4 kJ/(mol H_2)[74]) was reported for the equivalent dehydrogenation step. The enthalpy of reaction 1 corresponds to an equilibrium temperature much lower than the observed dehydrogenation onsets, substantiating that sluggish kinetics are governing the dehydrogenation of $Ca(BH_4)_2$-Mg_2NiH_4.

The experiments conducted to shed light on the reactivity between typical decomposition products of $Ca(BH_4)_2$ and Mg_2NiH_4 clearly show that the latter hydride or, more precisely, Mg_2Ni reacts with $CaB_{12}H_{12}$, CaB_6 and elemental boron (Fig. 4, Fig. 5 and Fig. 6). This is quite remarkable since especially $CaB_{12}H_{12}$ and elemental boron are rather stable and often considered as boron sinks that reduce reversibility in pure $Ca(BH_4)_2$ as well as in $Ca(BH_4)_2$ based hydride composites[27–29,32,35,37,75,71]. In all three mixtures, $MgNi_{2.5}B_2$ was created. This phase is the only boron containing compound in fully reacted Mg_2NiH_4-$CaB_{12}H_{12}$ and Mg_2NiH_4-CaB_6 (except for minor amounts of the initial reactants), see Fig. 4 and Fig. 5. As confirmed by the *in situ* SR-PXD experiments, also the dehydrogenation reaction paths of these two mixtures involve UP as intermediate phase. For that reason it seems reasonable to assume that UP is also an intermediate compound in the reaction of Mg_2NiH_4-B and can still be detected in the *ex situ* powder diffractogram due to the highly sluggish reaction kinetics. The hydrogenation experiments (Fig. 9, Fig. 10 and Fig. 11) clearly prove the possibility to form $Ca(BH_4)_2$ by absorbing material that only contains $MgNi_{2.5}B_2$ as sole boron donor. As a consequence, it is possible to produce $Ca(BH_4)_2$ from $CaB_{12}H_{12}$, CaB_6 and elemental boron *via* formation of $MgNi_{2.5}B_2$ as a transitional compound.

The systematic variation of the dehydrogenation temperature and time for the $Ca(BH_4)_2$-Mg_2NiH_4 composite revealed that there is indeed an influence of these two parameters on the composition and microstructure of the dehydrogenated materials and on the degree of reversibility (Fig. 7, Fig. 8 and Fig. 9). Independently of the dehydrogenation conditions and in accordance with reaction (3), the main chemical compounds of all desorbed samples are $MgNi_{2.5}B_2$, Mg and CaH_2. The temperature restriction to 350 °C leads to generally slower reaction kinetics (presence of unreacted $Ca(BH_4)_2$ after 150 min and 6 h) but seems also to promote the evolution of UP as an intermediate compound. This can be seen by comparing the relative intensities of UP reflections with those of $MgNi_{2.5}B_2$ in Fig. 7 a and in the *in situ* experiment (Fig. 1 a). If the temperature is limited to 350 °C, the following model appears to be the case: the ratio of UP formation and decomposition kinetics changes such that the net formation rate of this compound is enhanced. Moreover, also the kinetics of the reaction path directly leading to the formation of $MgNi_{2.5}B_2$ could be constrained even more by the temperature restriction. Reversely, $MgNi_{2.5}B_2$ forming reactions accelerate if the temperature is continuously increased to 450 °C which results in a lower peak concentration of UP. As it will be discussed separately, compared to the formation of $MgNi_{2.5}B_2$ the extent of solid state diffusion required for the formation of UP is probably smaller. Since diffusion coefficients increase with temperature, the same applies to the formation rate of $MgNi_{2.5}B_2$ – at the cost of diminished UP concentrations.

Besides $MgNi_{2.5}B_2$, all rehydrogenated samples comprise the crystalline phases MgH_2 and $Ca_4Mg_3H_{14}$ (Fig. 9 a). The first is formed directly from metallic Mg upon absorption, the latter is the product of the reaction between MgH_2 and CaH_2. Although $Ca(BH_4)_2$ was formed with an absorption yield of up to 20 % (Fig. 9 b), its reflections could not be detected (unambiguously) in the related PXD analyses (Fig. 9 a). Compared to the high reflection intensities of nickel containing compounds the scattering capability of $Ca(BH_4)_2$ is rather poor. However, the complete absence of detectable reflections certainly points towards particular microstructural properties

of $Ca(BH_4)_2$ such as small mean crystallite size or a high degree of disorder. Probably the formation of this hydride is confined in some way. The highest degrees of reversibility were obtained for the two samples initially dehydrogenated for 6 h at 350 °C and 450 °C, respectively. These results suggest that different properties of the desorbed samples need to be considered in order to explain the lower absorption yields of samples with shorter (150 min) and longer (42 h) desorption time. Typically, mean crystallite and particle sizes can have a significant influence on reaction kinetics. However, in this particular case no direct correlation between crystallite sizes and the degree of reversibility can be drawn as, for instance, the sample desorbed for 42 h at 350 °C features a significantly lower mean size of $MgNi_{2.5}B_2$ crystallites than the sample desorbed for 6 h at 450 °C. The latter showed the higher degree of reversibility, though. Thus, at this point no satisfying explanation can be provided based on the presented experimental results. As the processes upon rehydrogenation seem to be rather complex, more specific experiments need to be conducted.

Hydrogenation of $MgNi_{2.5}B_2$ with solely CaH_2 or MgH_2 addition was not successful (Fig. 10). The presence of both of the hydrides (or their respective cations) seems to be crucial for the formation of borohydrides in this system. Interestingly, in contrast to the initial assumption that the formation of $Ca_4Mg_3H_{14}$ upon reabsorption of the decomposition products of $Ca(BH_4)_2$-Mg_2NiH_2 could hinder further formation of $Ca(BH_4)_2$ and thus impede full absorption, the opposite seems to be the case as the two samples with $Ca_4Mg_3H_{14}$ as a starting reactant feature the best absorption yields. Hence, the increased equilibrium pressure for borohydride formation due to the presence of $Ca_4Mg_3H_{14}$ did not turn out to be an obstacle. Instead, activation energies of these samples appear to be rather low leading to higher degrees of absorption. These kinetic barriers are most likely related to solid state diffusion processes. Since all the three phases, i. e. $MgNi_{2.5}B_2$, CaH_2 and MgH_2, are required for the formation of $Ca(BH_4)_2$ the absorption reaction must take place at common interfaces of all three compounds. The further the reaction proceeds, the more diffusion of at least one of the components is necessary. If the desorbed state is prepared with $Ca_4Mg_3H_{14}$, the formation of $Ca(BH_4)_2$ will occur also at the interface of just the two phases $MgNi_{2.5}B_2$ and $Ca_4Mg_3H_{14}$. This can be seen directly for the sample $Ca_4Mg_3H_{14}$-$MgNi_{2.5}B_2$ that only features these two-phase-interfaces and still contains borohydrides after absorption. Within $Ca_4Mg_3H_{14}$ the two compounds CaH_2 and MgH_2 are virtually mixed on an atomic level whereby the extent of required solid state diffusion for borohydride formation at the interfaces with $MgNi_{2.5}B_2$ is minimized. In contrast to $Ca_4Mg_3H_{14}$-$MgNi_{2.5}B_2$-MgH_2 the sample without the addition of MgH_2 offers a worse absorption yield. This is due to the mismatch in stoichiometry as the Mg content in $Ca_4Mg_3H_{14}$ is just not high enough to allow for full absorption. It is noteworthy that upon hydrogenation of the two samples that were initially prepared with $Ca_4Mg_3H_{14}$ not only $Ca(BH_4)_2$ but also $Mg(BH_4)_2$ was formed. Since no $Mg(BH_4)_2$ could be detected after absorption of $MgNi_{2.5}B_2$-MgH_2 the presence of this borohydride must be directly related to $Ca_4Mg_3H_{14}$. Most likely $Mg(BH_4)_2$ is thermodynamically not stable in these systems but was formed as a metastable phase due to cation exchange reactions at the interface with $Ca_4Mg_3H_{14}$.

The preparation of the desorbed state material (BMH CaH_2-$MgNi_{2.5}B_2$-MgH_2) with strongly reduced particle size in order to enhance hydrogenation kinetics and improve the absorption yield was a great success (Fig. 11). Compared to all previous (re)hydrogenation attempts in which absorption yields of maximum 30 to 40 % were reached, the formation of $Ca(BH_4)_2$ was 2 to 3 times more effective in this experiment. Hence, the low mean particle sizes of the reactants clearly improved the absorption kinetics of this hydride composite. Since the amount of formed borohydride did not increase upon the second and third absorption step, all $Ca(BH_4)_2$ must have been created already in the very first absorption iteration. This is easily comprehensible in case of the sample that was solely hydrogenated without additional treatment (BMH, 3. abs. step, w/o intermediate milling). Here, already in the first absorption period, crystallite and particle sizes increased and inert interfaces were created by the newly formed phases. Due to these kinetic barriers, further absorption was hindered. Surprisingly, also the sample that was milled in between the individual absorption steps (BMH, 3rd abs. step, intermediate milling) did not feature an improved absorption yield compared to the reference specimen with just one absorption step (BMH, 1st abs. step). It appears that the impact of the comparatively short intermediate ball milling cycles was not enough in order to break inert structures and create new reactive interfaces of the residual reactants. Considering the low absorption yields of previous samples that were initially prepared by 300 min of ball milling in the Spex mill, the insignificant influence of the intermediate milling cycles on the formation of $Ca(BH_4)_2$ is consistent. The milling had an impact on the microstructure of $Ca(BH_4)_2$, though. The shift of the resonance as well as the increased peak width is caused by a polymorphous change. The resonance peak is, in fact, a superposition of the two resonances of α- and β-$Ca(BH_4)_2$ at -30 ppm and -32 ppm, respectively[27,32]. Typically, β-$Ca(BH_4)_2$ is the stable modification above approximately 175 °C.[23,65,67] In this experiment, β-$Ca(BH_4)_2$ was partially stabilised at low temperatures as a consequence of the intermediate milling treatment. Furthermore, the increased relative intensity of the spinning side bands of $Ca(BH_4)_2$ must be attributed to a reduction of crystallite sizes as well as an increment of crystal defects due to the milling. The presented results not only imply that absorption of as-milled BMH basically occurred in the first hydrogenation step but also that the formation of $Ca(BH_4)_2$ must have stopped rather early. This becomes evident when considering also the second hydrogenation of as-milled BHM (2. BMH, 1. abs. step). At 87 % this sample features a significantly higher absorption yield than the reference sample (BMH, 1. abs. step). However, this improvement cannot simply be attributed to higher hydrogen pressure in general because also during the second and third absorption step of the first hydrogenation routine the pressure rose to 420 bar. It appears

rather unlikely that the pressure increment from 420 bar to 440 bar could boost the absorption yield to such an extent, especially since this composite's equilibrium pressure at 400 °C must be lower than 310 bar. The particular difference between the first and the second hydrogenation of as-milled BMH was that in case of the latter already upon heating up and also during the first period at maximum temperature the gas pressure was considerably higher. Consequently, the stronger driving force could promote reaction kinetics and lead to an improved conversion within the same timeframe. The dwell time at 400 °C seems to be an important factor for the absorption process. The longer the powder is kept at this temperature the more its crucial properties (very small crystallite and particle sizes, high number of defects and dislocations) induced by the intense milling process vanish and growing kinetic constraints hinder further hydrogenation. Therefore, additional absorption time – in this experiment further absorption steps – do not improve the absorption yield.

The variety of results also provides important information on $MgNi_{2.5}B_2$. These allow to draw conclusions about structural properties and the reactivity of this compound. The crystal structure of $MgNi_{2.5}B_2$ was characterised for the first time by Jung in 1977[55]. He described the ternary boride as hexagonal crystal with the space group $P6_222$ (No. 180). Ni atoms are located at the Wyckoff sites 3*d* and 6*f*, most of the Mg atoms at 3*a* and the B atoms at site 6*i*. However, about one quarter of the Mg atoms occupy as well 3*d* and 6*f* sites. Therefore, these sites are partially occupied by both Ni and Mg; the total occupancies are yet only 89 % (3*d*) and 93 % (6*f*). In addition, Jung pointed out that single phase diffractograms can also be obtained for slightly different atomic compositions indicating that $MgNi_{2.5}B_2$ features a certain homogeneity range. Since the measured cell parameters are practically independent from these changes of the atomic composition, Jung explained his results by modifications of the total and partial occupancies of the Wyckoff sites. This assumption is supported by a publication of Gross et al.[56] from 1998. The authors reported the crystal structure of $MgNi_3B_2$. This compound has the same cell parameters and space group as Jung's structure. In contrast to the latter, $MgNi_3B_2$ exhibits no substitution of Ni by Mg on the 3*d* and 6*f* sites. Moreover, all sites are fully occupied. The authors used a different synthesis method as compared to Jung. Hence, it seems the structure and atomic composition of $MgNi_{2.5}B_2$ (i. e. the site occupancies and the distribution of atoms) are not fixed but depend on the way this compound is formed. Consequently, for the $Ca(BH_4)_2$-Mg_2NiH_4 system the experimental conditions (desorption temperature, time and hydrogen pressure as well as the type of boron donor) determine not only the reaction path and kinetics but also the state of the formed $MgNi_{2.5}B_2$. The existence of a homogeneity range for $MgNi_{2.5}B_2$ is supported by the presented PXD analyses. For instance, the comparison of the $MgNi_{2.5}B_2$ diffraction pattern in Fig. 4 and Fig. 7 reveals obvious differences. Although the positions of the Bragg reflections match, the corresponding intensities vary to some degree pointing towards altered scattering capabilities of the Wyckoff sites (modified occupancies and/or substitutional effects). In addition, the diffractograms of the five rehydrogenated specimens (Fig. 9 a) contain valuable information. By means of the Rietveld method the mass fractions of the diffractive compounds were evaluated. All samples show rather similar values that are in good agreement with the theoretical mass fractions that would be expected if only MgH_2 and $Ca_4Mg_3H_{14}$ were formed in the absorption process (56.7 mass%, 25.1 mass% and 18.2 mass% for $MgNi_{2.5}B_2$, MgH_2 and $Ca_4Mg_3H_{14}$, respectively). This applies also to the reabsorbed sample initially dehydrogenated at 350 °C for 6 h. However, the ^{11}B NMR spectrum (Fig. 9 b) of this sample reveals that about 20 % of the boron is bonded in $Ca(BH_4)_2$. Thus, one would expect to find the corresponding 20 % of Mg and Ni from $MgNi_{2.5}B_2$ in another chemical state. Besides $MgNi_{2.5}B_2$ no other Ni-containing phases can be identified, though. That includes especially Mg_2Ni and Mg_2NiH_4 as well as $MgNi_2$ and elemental Ni. This observation might be ascribed to the homogeneity range of $MgNi_{2.5}B_2$, too. Since 20 % of the boron initially bonded in $MgNi_{2.5}B_2$ was transferred to $Ca(BH_4)_2$ without formation of additional Ni-containing compounds, the occupancy of the boron site 6*i* in the $MgNi_{2.5}B_2$ crystal must be reduced to roughly 0.8. The homogeneous reduction of the boron concentration in $MgNi_{2.5}B_2$ requires a certain mobility of boron atoms within the crystal. For a long range diffusion of boron vacancies two different interatomic distances of 1.94 Å and 3.02 Å need to be overcome alternatingly. Hence, solely from this structural point of view a reasonable mobility of boron atoms in $MgNi_{2.5}B_2$ seems possible. A reduction of the boron concentration by 20 % in $MgNi_{2.5}B_2$ would certainly affect the diffraction pattern of this phase. However, since the atomic form factor of boron is rather small compared the one of Mg and especially the one of Ni, the impact of a reduced occupancy of site 6*i* on the reflection intensities would be relatively low. In fact, the intensities of the four most intense peaks, i. e. the (200), (103), (100) and (104) reflections, would be changed by only 0.7 %, 4.3 %, -8.8 % and -2.1 %, respectively. Moreover, the (100) reflection which would be affected the most by this structural modification is superimposed by the broad background peak caused by the PMMA dome used for the *ex situ* diffraction experiments. Therefore, an experimental confirmation of the reduced boron occupancy in $MgNi_{2.5}B_2$ cannot be provided due to the resolution limit of the laboratory diffractometer.

Moreover, it should be noticed that the measured chemical shifts of $MgNi_{2.5}B_2$ differ significantly for the different experiments (Fig. 3, Fig. 5 and Fig. 7 b). The respective centre band positions range from 142 ppm to 168 ppm. Furthermore, the shape of the $MgNi_{2.5}B_2$ ^{11}B NMR resonance varies noticeably for the different dehydrogenation conditions (Fig. 3 and Fig. 7 b). These observations provide additional evidence for the variations in the crystal structure of this ternary boride and thus for the existence of the discussed homogeneity range. Interestingly, if the as-synthesised $MgNi_{2.5}B_2$ is regarded as a reference material – the NMR signal of this compound can be seen in Fig. 10 – the $MgNi_{2.5}B_2$ formed upon desorption at a

hydrogen pressure of 50 bar (Fig. 3) certainly shows the closest resemblance. Independent of the temperature, a chemical shift of 142 ppm was determined in all these samples. This value is almost identical to the chemical shift measured for the as-synthesized $MgNi_{2.5}B_2$ (141 ppm). In contrast to the spectra of all samples desorbed at 1 bar H_2, considerably lower widths and higher symmetries of the $MgNi_{2.5}B_2$ resonance signal can be recognised in case of the specimens dehydrogenated at 50 bar. Also these characteristics are very similar to the reference material. As discussed earlier, at 50 bar H_2 the two hydrides $Ca(BH_4)_2$ and Mg_2NiH_4 react mutually. Especially the formation of Mg_2Ni – which seems to be an essential reactant for the formation of UP – is avoided. Obviously, the altered reaction path at high hydrogen pressures facilitates the development of a more homogenous micro- and crystal structure of $MgNi_{2.5}B_2$ which leads to the rather sharp resonance peak at the well-defined chemical shift of 142 ppm. In case of the as-synthesised $MgNi_{2.5}B_2$ the high temperature of 930 °C might be the reason for a similarly ordered and homogeneous state.

It is possible that the particular crystal structure of $MgNi_{2.5}B_2$ also affects the rehydrogenation kinetics and thus the degree of reversibility of $Ca(BH_4)_2$-Mg_2NiH_4. However, as set out above the state of the formed $MgNi_{2.5}B_2$ depends on many experimental parameters. As a consequence, a systematic control of the crystal structure appears very difficult or even impossible. Therefore, the influence of the $MgNi_{2.5}B_2$ crystal structure on the reversibility of the system could not be investigated in an isolated way.

The presented PXD and NMR analyses contain sufficient information to obtain a first quantitative estimate for the chemical composition of UP. Besides the reflections of $MgNi_{2.5}B_2$ and UP the diffractogram of reacted Mg_2NiH_4-B in Fig. 4 shows neither peaks of Mg_2Ni nor any other Ni containing phase although roughly 28 % of boron remained unreacted (proven by the respective ^{11}B spectrum in Fig. 5) and the ratio of Mg_2NiH_4 and boron was chosen exactly to meet the atomic ratio of Ni and boron in $MgNi_{2.5}B_2$. The Rietveld refinement of this diffractogram – computed on those sections that do not contain reflections of UP – revealed a $MgNi_{2.5}B_2$ to Mg weight ratio of about 72:28. The corresponding values for reacted Mg_2NiH_4-$CaB_{12}H_{12}$ and Mg_2NiH_4-CaB_6 are 75:25 and 72:28, respectively. These three ratios are very similar although (almost) full boron transfer to $MgNi_{2.5}B_2$ only occurred in case of the latter two samples. This implies that all or at least the majority of Mg in reacted Mg_2NiH_4-B was released as a by-product of the $MgNi_{2.5}B_2$ formation. Consequently, for the formation of UP from the reactants Mg_2NiH_4 and B no or just very minor amounts of Mg are consumed or set free. Therefore the atomic ratio of Mg and Ni in UP must be equal or close to 2:1.

The three ratios slightly differ from the theoretical weight ratio of $MgNi_{2.5}B_2$ and Mg of 67:33 that is expected to be present in all samples if boron is transferred exclusively to $MgNi_{2.5}B_2$. This small deviation might be caused by differences between the actual atomic composition of $MgNi_{2.5}B_2$ obtained under these experimental conditions and the structure/composition introduced by the CIF file (based on Jung's publication[55]) used for the refinements. In other words, the structural freedom of $MgNi_{2.5}B_2$ due to the homogeneity range was not taken into account at this point. Furthermore, the total atomic ratio of Ni and B in the sample Mg_2NiH_4-B equals 2.5:2. Since all Ni is either bonded in $MgNi_{2.5}B_2$ or UP but about 28 % of boron remained in the elemental state, the atomic ratio of Ni and B in UP must be greater than 2.5:2. These considerations can be expressed in the following chemical equation (here assuming the atomic ratio of Mg and Ni in UP to be exactly 2:1):

$$2.5Mg_2NiH_4 + 2B \rightarrow 2.5Mg_2Ni + 2B + 5H_2\uparrow$$

$$= x(2.5Mg_2Ni + 2B) + (1-x)(2.5Mg_2Ni + 2yB + 2(1-y)B)$$

$$\rightarrow x(MgNi_{2.5}B_2 + 4Mg) + (1-x)\left(Mg_5Ni_{2.5}B_{2y} + 2(1-y)B\right)$$

$$= xMgNi_{2.5}B_2 + 4xMg + (1-x)\underbrace{Mg_5Ni_{2.5}B_{2y}}_{\approx UP} + 2\underbrace{(1-x)(1-y)}_{\approx 0.28}B$$

, with $x, y \in]0,1[$.

Unfortunately, it is not possible to determine x and y because a second boundary condition cannot be extracted from the experimental results. Since UP is an intermediate phase in the reaction between a boron donor and Mg_2Ni to $MgNi_{2.5}B_2$, the estimated atomic composition of UP appears plausible. The ratio of Mg and Ni is similar or equal to the one in Mg_2Ni and the relative boron content is lower than the one in $MgNi_{2.5}B_2$. Considering that solid state diffusion is often the rate limiting step in solid-solid reactions, the formation of thermodynamically less favourable, intermediate phases might occur that require less atomic diffusion. Comparing the atomic compositions of $MgNi_{2.5}B_2$ and UP, the necessary extent of solid state diffusion to form the latter compound from the described starting reactants is certainly smaller. Interestingly, the ^{11}B NMR spectrum of reacted Mg_2NiH_4-B only appears to exhibit the resonances of $MgNi_{2.5}B_2$ and boron. No other distinct signals could be resolved. Therefore the resonance of UP seems to overlap with the one of $MgNi_{2.5}B_2$. Hence, the electronic structures with respect to boron must to be rather similar in these two compounds.

Conclusions

The dehydrogenation reaction path of the Reactive Hydride Composite $Ca(BH_4)_2$-Mg_2NiH_4 strongly depends on the applied hydrogen back pressure. Independently from this pressure, only CaH_2, $MgNi_{2.5}B_2$ and Mg are present after full dehydrogenation. Three consecutive reaction steps can be distinguished. The first step that can be observed at hydrogen pressures higher than (at least) 7.5 bar appears to be a concerted reaction between $Ca(BH_4)_2$ and Mg_2NiH_4 forming the three dehydrogenation products $Ca_4Mg_3H_{14}$, $MgNi_{2.5}B_2$ and

MgH_2. This reaction occurs at temperatures lower than the dehydrogenation temperatures of pure $Ca(BH_4)_2$ and Mg_2NiH_4 confirming the mutual destabilisation between the two hydrides. By means of DSC analyses, the enthalpy of this concerted reaction could be estimated to about 15 kJ/(mol H_2). At lower hydrogen pressures the dehydrogenation of the composite starts with the desorption of Mg_2NiH_4 under formation of Mg_2Ni. The presence of this intermetallic enables a side reaction with $Ca(BH_4)_2$ and/or its dehydrogenation products forming an intermediate Mg-Ni-B phase (UP). The composition of this yet unknown ternary compound could be estimated to Mg:Ni:B ≈ 2:1:x, x < 0.8. In addition, $MgNi_{2.5}B_2$ was successfully synthesised from Mg_2NiH_4 and each of the three typical boron containing decomposition products of $Ca(BH_4)_2$, i. e. CaB_6, $CaB_{12}H_{12}$ and elemental boron. Consequently, these compounds cannot be found (in larger quantities) among the reaction products of $Ca(BH_4)_2$-Mg_2NiH_4 after full dehydrogenation. $CaB_{12}H_{12}$ and elemental boron are usually considered as stable boron sinks that hinder (full) reversibility of $Ca(BH_4)_2$ and its respective composites. Hence, the possibility to transfer boron from these compounds to another phase ($MgNi_{2.5}B_2$) that is capable to donate the boron for $Ca(BH_4)_2$ formation must be considered as important discovery for the utilisation of $Ca(BH_4)_2$ as a reversible hydrogen storage medium. Although reversibility of $Ca(BH_4)_2$-Mg_2NiH_4 is rather limited without special treatment due to slow solid state diffusion processes, an absorption yield of about 87 % was reached by intense milling prior to the hydrogenation procedure.

Acknowledgements

This work was supported by the Danish Council for Strategic Research via HyFillFast. Access to beam time at the synchrotron PETRA III at DESY, Hamburg, Germany is gratefully acknowledged.

Notes and references

1 T. M. I. Mahlia, T. J. Saktisahdan, A. Jannifar, M. H. Hasan and H. S. C. Matseelar, *Renew. Sustain. Energy Rev.*, 2014, **33**, 532–545.

2 B. Zakeri and S. Syri, *Renew. Sustain. Energy Rev.*, 2015, **42**, 569–596.

3 B. Zakeri and S. Syri, *Renew. Sustain. Energy Rev.*, 2015, **53**, 1634–1635.

4 M. A. Pellow, C. J. M. Emmott, C. J. Barnhart and S. M. Benson, *Energy Environ. Sci.*, 2015, **8**, 1938–1952.

5 L. Schlapbach and A. Züttel, *Nature*, 2001, **414**, 353–358.

6 S. Orimo, Y. Nakamori, J. R. Eliseo, A. Züttel and C. M. Jensen, *Chem. Rev.*, 2007, **107**, 4111–4132.

7 Q. Lai, M. Paskevicius, D. A. Sheppard, C. E. Buckley, A. W. Thornton, M. R. Hill, Q. Gu, J. Mao, Z. Huang, H. K. Liu, Z. Guo, A. Banerjee, S. Chakraborty, R. Ahuja and K. F. Aguey-Zinsou, *ChemSusChem*, 2015, **8**, 2789–2825.

8 K. T. Møller, T. R. Jensen, E. Akiba and H. Li, *Prog. Nat. Sci. Mater. Int.*, 2017, **27**, 34–40.

9 B. Bogdanović and M. Schwickardi, *J. Alloys Compd.*, 1997, **253–254**, 1–9.

10 P. Chen, Z. Xiong, J. Luo, J. Lin and K. L. Tan, *Nature*, 2002, **420**, 302–304.

11 G. Barkhordarian, T. Klassen and R. Bormann, 2005, patent CA2590210 A1.

12 G. Barkhordarian, T. Klassen, M. Dornheim and R. Bormann, *J. Alloys Compd.*, 2007, **440**, L18–L21.

13 J. J. Vajo, S. L. Skeith and F. Mertens, *J. Phys. Chem. B*, 2005, **109**, 3719–3722.

14 H. W. Li, Y. Yan, S. I. Orimo, A. Züttel and C. M. Jensen, *Energies*, 2011, **4**, 185–214.

15 M. B. Ley, L. H. Jepsen, Y. S. Lee, Y. W. Cho, J. M. Bellosta Von Colbe, M. Dornheim, M. Rokni, J. O. Jensen, M. Sloth, Y. Filinchuk, J. E. Jørgensen, F. Besenbacher and T. R. Jensen, *Mater. Today*, 2014, **17**, 122–128.

16 L. H. Rude, T. K. Nielsen, D. B. Ravnsbæk, U. Bösenberg, M. B. Ley, B. Richter, L. M. Arnbjerg, M. Dornheim, Y. Filinchuk, F. Besenbacher and T. R. Jensen, *Phys. Status Solidi Appl. Mater. Sci.*, 2011, **208**, 1754–1773.

17 M. Paskevicius, L. H. Jepsen, P. Schouwink, R. Černý, D. B. Ravnsbæk, Y. Filinchuk, M. Dornheim, F. Besenbacher and T. R. Jensen, *Chem. Soc. Rev.*, 2017, **46**, 1565–1634.

18 R. Mohtadi, M. Matsui, T. S. Arthur and S. J. Hwang, *Angew. Chemie - Int. Ed.*, 2012, **51**, 9780–9783.

19 R. Mohtadi and S. Orimo, *Nat. Rev. Mater.*, 2016, **2**, 16091.

20 M. Felderhoff and B. Bogdanović, *Int. J. Mol. Sci.*, 2009, **10**, 325–344.

21 E. C. E. Rönnebro, G. Whyatt, M. Powell, M. Westman, F. Zheng and Z. Z. Fang, *Energies*, 2015, **8**, 8406–8430.

22 R. Mohtadi, A. Remhof and P. Jena, *J. Phys. Condens. Matter*, 2016, **28**, 353001.

23 E. Rönnebro and E. H. Majzoub, *J. Phys. Chem. B*, 2007, **111**, 12045–12047.

24 J. H. Kim, S. A. Jin, J. H. Shim and Y. W. Cho, *J. Alloys Compd.*, 2008, **461**, L20–L22.

25 J. Y. Lee, D. Ravnsbæk, Y.-S. Lee, Y. Kim, Y. Cerenius, J.-H. Shim, T. R. Jensen, N. H. Hur and Y. W. Cho, *J. Phys. Chem. C*, 2009, **113**, 15080–15086.

26 F. Pendolino, *J. Phys. Chem. C*, 2012, **116**, 1390–1394.

27 Y. Yan, A. Remhof, D. Rentsch, A. Züttel, S. Giri and P. Jena, *Chem. Commun.*, 2015, **51**, 11008–11011.

28 C. Bonatto Minella, S. Garroni, C. Pistidda, R. Gosalawit-Utke, G. Barkhordarian, C. Rongeat, I. Lindemann, O. Gutfleisch, T. R. Jensen, Y. Cerenius, J. Christensen, M. D. Baró, R. Bormann, T. Klassen and M. Dornheim, *J. Phys. Chem. C*, 2011, **115**, 2497–2504.

29 Y. Kim, D. Reed, Y. S. Lee, J. Y. Lee, J. H. Shim, D. Book and Y. W. Cho, *J. Phys. Chem. C*, 2009, **113**, 5865–5871.

30 V. Ozolins, E. H. Majzoub and C. Wolverton, *J. Am. Chem. Soc.*, 2009, **131**, 230–237.

31 Y. Zhang, E. Majzoub, V. Ozoliņš and C. Wolverton, *Phys. Rev. B - Condens. Matter Mater. Phys.*, 2010, **82**, 174107.

32 Y. Kim, S. J. Hwang, J. H. Shim, Y. S. Lee, H. N. Han and Y. W. Cho, *J. Phys. Chem. C*, 2012, **116**, 4330–4334.

33 Y. Kim, S. J. Hwang, Y. S. Lee, J. Y. Suh, H. N. Han and Y. W.

Cho, *J. Phys. Chem. C*, 2012, **116**, 25715–25720.
34 C. J. Sahle, C. Sternemann, C. Giacobbe, Y. Yan, C. Weis, M. Harder, Y. Forov, G. Spiekermann, M. Tolan, M. Krisch and A. Remhof, *Phys. Chem. Chem. Phys.*, 2016, **18**, 19866–19872.
35 Y. Yan, D. Rentsch and A. Remhof, *Phys. Chem. Chem. Phys.*, 2017, **19**, 7788–7792.
36 C. B. Minella, C. Pistidda, S. Garroni, P. Nolis, M. D. Baró, O. Gutfleisch, T. Klassen, R. Bormann and M. Dornheim, *J. Phys. Chem. C*, 2013, **117**, 3846–3852.
37 C. Bonatto Minella, S. Garroni, D. Olid, F. Teixidor, C. Pistidda, I. Lindemann, O. Gutfleisch, M. D. Baró, R. Bormann, T. Klassen and M. Dornheim, *J. Phys. Chem. C*, 2011, **115**, 18010–18014.
38 F. Karimi, P. Klaus Pranzas, C. Pistidda, J. A. Puszkiel, C. Milanese, U. Vainio, M. Paskevicius, T. Emmler, A. Santoru, R. Utke, M. Tolkiehn, C. B. Minella, A.-L. Chaudhary, S. Boerries, C. E. Buckley, S. Enzo, A. Schreyer, T. Klassen and M. Dornheim, *Phys. Chem. Chem. Phys.*, 2015, **17**, 27328–27342.
39 J. Huang, M. Gao, Z. Li, X. Cheng, J. Gu, Y. Liu and H. Pan, *J. Alloys Compd.*, 2016, **670**, 135–143.
40 H. Chu, Z. Xiong, G. Wu, J. Guo, X. Zheng, T. He, C. Wu and P. Chen, *Chem. - An Asian J.*, 2010, **5**, 1594–1599.
41 N. Poonyayant, V. Stavila, E. H. Majzoub, L. E. Klebanoff, R. Behrens, N. Angboonpong, M. Ulutagay-Kartin, P. Pakawatpanurut, E. S. Hecht and J. S. Breit, *J. Phys. Chem. C*, 2014, **118**, 14759–14769.
42 B. R. S. Hansen, K. T. Møller, M. Paskevicius, A.-C. Dippel, P. Walter, C. J. Webb, C. Pistidda, N. Bergemann, M. Dornheim, T. Klassen, J.-E. Jørgensen and T. R. Jensen, *J. Appl. Crystallogr.*, 2015, **48**, 1234–1241.
43 U. Bösenberg, C. Pistidda, M. Tolkiehn, N. Busch, I. Saldan, K. Suarez-Alcantara, A. Arendarska, T. Klassen and M. Dornheim, *Int. J. Hydrogen Energy*, 2014, **39**, 9899–9903.
44 A. P. Hammersley, *ESRF Intern. Rep.*, 1997, **ESRF97HA02**.
45 A. P. Hammersley, S. O. Svensson, M. Hanfland, A. N. Fitch and D. Hausermann, *High Press. Res.*, 1996, **14**, 235–248.
46 *http://maud.radiographema.com, accessed on 2017-06-16*.
47 L. Lutterotti, *Nucl. Instruments Methods Phys. Res. Sect. B Beam Interact. with Mater. Atoms*, 2010, **268**, 334–340.
48 J. J. Reilly and R. H. J. Wiswall, *Inorg. Chem.*, 1968, **7**, 2254–2256.
49 Z. Gavra, M. H. Mintz, G. Kimmel and Z. Hadari, *Inorg. Chem.*, 1979, **18**, 3595–3597.
50 D. Noréus and L. G. Olsson, *J. Chem. Phys.*, 1983, **78**, 2419.
51 P. Zolliker, K. Yvon and C. H. Baerlocher, *J. Less Common Met.*, 1986, **115**, 65–78.
52 D. Noréus and L. Kihlborg, *J. Less Common Met.*, 1986, **123**, 233–239.
53 K. Zeng, T. Klassen, W. Oelerich and R. Bormann, *J. Alloys Compd.*, 1999, **283**, 213–224.
54 B. Ao, Z. Zhang, Y. He and Y. Zhao, *Int. J. Hydrogen Energy*, 2013, **38**, 16471–16476.
55 W. Jung, *Zeitschrift für Naturforsch. B*, 1977, **32**, 1371–1374.
56 K. J. Gross, A. Züttel and L. Schlapbach, *J. Alloys Compd.*, 1998, **274**, 234–238.
57 P. Manfrinetti, M. Pani, S. K. Dhar and R. Kulkarni, *J. Alloys Compd.*, 2007, **428**, 94–98.
58 F. Gingl, F. Bonhomme, K. Yvon and P. Fischer, *J. Alloys Compd.*, 1992, **185**, 273–278.
59 K. Yvon and B. Bertheville, *J. Alloys Compd.*, 2006, **425**, 101–108.
60 S. Djellab, Y. Bouhadda, M. Bououdina, N. Fenineche and Y. Boudouma, *J. Electron. Mater.*, 2016, **45**, 3935–3942.
61 V. Bérubé, G. Radtke, M. Dresselhaus and G. Chen, *Int. J. Energy Res.*, 2007, **31**, 637–663.
62 R. A. Varin, L. Zbroniec, M. Polanski and J. Bystrzycki, *Energies*, 2011, **4**, 1–25.
63 R. Janot and D. Guerard, *Prog. Mater. Sci.*, 2005, **50**, 1–92.
64 C. Wall, A. Pohl, M. Knapp, H. Hahn and M. Fichtner, *Powder Technol.*, 2014, **264**, 409–417.
65 N. Bergemann, C. Pistidda, C. Milanese, T. Emmler, F. Karimi, A.-L. Chaudhary, M. R. Chierotti, T. Klassen and M. Dornheim, *Chem. Commun.*, 2016, **52**, 4836–4839.
66 E. H. Majzoub and E. Rönnebro, *J. Phys. Chem. C*, 2009, **113**, 3352–3358.
67 Y. Filinchuk, E. Rönnebro and D. Chandra, *Acta Mater.*, 2009, **57**, 732–738.
68 W. Li, J. J. Vajo, R. W. Cumberland, P. Liu, S. J. Hwang, C. Kim and R. C. Bowman, *J. Phys. Chem. Lett.*, 2010, **1**, 69–72.
69 G. Barkhordarian, T. R. Jensen, S. Doppiu, U. Bösenberg, A. Borgschulte, R. Gremaud, Y. Cerenius, M. Dornheim, T. Klassen and R. Bormann, *J. Phys. Chem. C*, 2008, **112**, 2743–2749.
70 B. Schiavo, A. Girella, F. Agresti, G. Capurso and C. Milanese, *J. Alloys Compd.*, 2011, **509**, S714–S718.
71 C. Pistidda, F. Karimi, S. Garroni, A. Rzeszutek, C. Bonatto Minella, C. Milanese, T. T. Le, L. H. Rude, J. Skibsted, T. R. Jensen, C. Horstmann, C. Gundlach, M. Tolkiehn, P. K. Pranzas, A. Schreyer, T. Klassen and M. Dornheim, *J. Phys. Chem. C*, 2014, **118**, 28409–28417.
72 H. W. Li, E. Akiba and S. I. Orimo, *J. Alloys Compd.*, 2013, **580**, S292–S295.
73 Z. Łodziana, P. Błoński, Y. Yan, D. Rentsch and A. Remhof, *J. Phys. Chem. C*, 2014, **118**, 6594–6603.
74 J. J. Vajo, W. Li and P. Liu, *Chem. Commun.*, 2010, **46**, 6687.
75 C. Bonatto Minella, S. Garroni, C. Pistidda, M. D. Baró, O. Gutfleisch, T. Klassen and M. Dornheim, *J. Alloys Compd.*, 2015, **622**, 989–994.

